Available online at www.sciencedirect.com

SciVerse ScienceDirect

Geochimica et Cosmochimica Acta 100 (2013) 41–59

Geochimica et Cosmochimica Acta

www.elsevier.com/locate/gca

Disequilibrium melting and melt migration driven by impacts: Implications for rapid planetesimal core formation

Andrew G. Tomkins *, Roberto F. Weinberg, Bruce F. Schaefer [1], Andrew Langendam

School of Geosciences, P.O. Box 28E, Monash University, Melbourne, Victoria 3800, Australia

Received 20 January 2012; accepted in revised form 24 September 2012; available online 12 October 2012

Abstract

The $\varepsilon^{182}W$ ages of magmatic iron meteorites are largely within error of the oldest solar system particles, apparently requiring a mechanism for segregation of metals to the cores of planetesimals within 1.5 million years of initial condensation. Currently favoured models involve equilibrium melting and gravitational segregation in a static, quiescent environment, which requires very high early heat production in small bodies via decay of short-lived radionuclides. However, the rapid accretion needed to do this implies a violent early accretionary history, raising the question of whether attainment of equilibrium is a valid assumption. Since our use of the Hf–W isotopic system is predicated on achievement of chemical equilibrium during core formation, our understanding of the timing of this key early solar system process is dependent on our knowledge of the segregation mechanism. Here, we investigate impact-related textures and microstructures in chondritic meteorites, and show that impact-generated deformation promoted separation of liquid FeNi into enlarged sulfide-depleted accumulations, and that this happened under conditions of thermochemical disequilibrium. These observations imply that similar enlarged metal accumulations developed as the earliest planetesimals grew by rapid collisional accretion. We suggest that the nonmagmatic iron meteorites formed this way and explain why they contain chondritic fragments in a way that is consistent with their trace element characteristics. As some planetesimals grew large enough to develop partially molten silicate mantles, these enlarged metal accumulations would settle rapidly to form cores leaving sulfide and small metal particles behind, since gravitational settling rate scales with the square of metal particle size. Our model thus provides a mechanism for more rapid core formation with less radiogenic heating. In contrast to existing models of core formation, the observed rarity of sulfide-dominant meteorites is an expected consequence of our model, which promotes early and progressive separation of metal and sulfide. We suggest that the core formation models that assume attainment of equilibrium in the Hf–W system underestimate the core formation time.

1. INTRODUCTION

Magmatic iron meteorites are thought to represent the cores of planetesimals (Wasson and Richardson, 2001; Chabot and Haack, 2006; Schersten et al., 2006). Their tungsten isotope signatures have been interpreted as indicating that cores formed within 1.5 million years of the oldest solar system particles (Bizzaro et al., 2005; Carlson and Boyet, 2009; Kleine et al., 2009; Kruijer et al., 2012). However, these ages assume that cores formed by equilibrium fractionation of metal from silicate, which is problematic given the implied rapidity of core formation. In the more widely accepted core formation models, immiscible globules of Fe–Ni–S melt either settled through a partially molten silicate mantle (cf. Stevenson, 1990; McCoy et al., 2006; Wood et al., 2006; Sahijpal et al., 2007; Bagdassarov et al., 2009), or migrated through percolative flow (Yoshino et al., 2003, 2004; Roberts et al., 2007), allowing equilibrium partitioning of siderophile and lithophile elements. A third model suggests that impacts may have played a role in driving melt

* Corresponding author. Tel.: +61 3 99051643; fax: +61 3 99054903.

E-mail address: andy.tomkins@monash.edu (A.G. Tomkins).

[1] Present address: GEMOC, Earth and Planetary Sciences, Macquarie University, NSW 2109, Australia.

0016-7037/$ - see front matter © 2012 Elsevier Ltd. All rights reserved.
http://dx.doi.org/10.1016/j.gca.2012.09.044

migration (Bruhn et al., 2000; Rushmer et al., 2005), which could happen on a comparatively rapid timescale and may not require a silicate magma ocean, or complete equilibration between metal and silicate. Incomplete equilibration between segregating metal and silicate would result in mantle excess of ^{182}W, and thus the ages derived from isotopic analysis of iron meteorites would underestimate the core formation time (Nimmo and Agnor, 2006). Thus understanding whether planetesimal cores formed by an equilibrium, or partial disequilibrium, process is critical to our understanding of the temporal evolution of the early solar system.

Here, we investigate processes that controlled formation of enlarged metal accumulations within ordinary chondrite (OC) meteorites. The parent bodies for these meteorites are thought to have formed approximately 2–3 million years. after CAIs (e.g., see Harrison and Grimm, 2010). Thermal metamorphism in the early solar system is thought to have been dominantly caused by radiogenic heating through decay of ^{26}Al and ^{60}Fe (e.g., Moskovitz and Gaidos, 2011), and since the half lives of these isotopes are only 0.717 and 1.5 million years respectively, the OC meteorites escaped the most intense period of radiogenic heating. Although radiogenic metamorphism generated temperatures that may have significantly exceeded 900 °C near the cores of the OC parent bodies (e.g., Harrison and Grimm, 2010), they are thought to have escaped widespread metal–troilite melting (Slater-Reynolds and McSween, 2005), and this is certainly true for less metamorphosed petrologic types (types 3–5). The OC meteorites thus preserve the effects of impacts on metal–sulfide–silicate assemblages, without having been overprinted by melting associated with radiogenic metamorphism, and are consequently our best record of these processes.

In OC meteorites, many researchers have observed silicate glasses in veins and breccias, which formed through localised impact heating during collisions between asteroids (Stoffler et al., 1991). Encapsulated within these silicate glasses are typically numerous micro- to nano-scale spherical balls of FeNi metal and/or troilite (FeS), indicating that these components were also melted during impacts and then trapped as immiscible melt globules in the silicate melt. Micro-scale metal ± troilite veinlets have also been observed in these meteorites, and it is generally accepted that they represent trapped metal and/or troilite melt (Stoffler et al., 1991). Rare OC meteorites contain significantly thicker (mm- to cm-scale) metal-dominated veins, or metal-cemented breccias (Rubin et al., 2001; Ruzicka et al., 2005). This metal enrichment is thought to be the result of migration of immiscible metal ± sulfide melts generated by impact heating (Rubin et al., 2001; Ruzicka et al., 2005). However, the specific processes responsible for preferential migration and accumulation of metal melt over sulfide melt, and particularly over silicate melt, have not been clearly demonstrated.

In this study, we start by investigating the physical drivers responsible for this preferential metal migration by examining the structural setting of metal and troilite veins in impact-affected OC meteorites. Because these controlling mechanisms are based on physical principles that apply to any solid body that contains a metal–sulfide–silicate assemblage, the findings apply to asteroids and planetesimals that formed before the OC parent bodies. This principle allows us to investigate how impacts in the earliest solar system might have influenced the process of core formation, and generate insights into the consequences for the global-scale geochemistry of planetesimals and ultimately, planets.

2. OBSERVED FEATURES OF IMPACT-INDUCED MELTING AND METAL/SULFIDE MELT MIGRATION

The dominant majority of OC meteorites have been affected by shock caused by hypervelocity collisions on their parent bodies. A well-accepted petrographic classification scheme (Stoffler et al., 1991) has been used by scientists to divide numerous OC meteorites into six classes reflecting increasing intensity of shock from S1 to S6. In this section, an overview of melt-bearing features attributed to impact processes is provided, progressing from micro- to macro-scale, highlighting key aspects that will facilitate discussion on drivers of melt segregation and associated disequilibrium in subsequent sections.

2.1. Isolated melt pockets

Initial signs of shock-induced melting are recognised in moderately impact-affected meteorites that have characteristics of shock Stages S3 and S4. In these meteorites, isolated melt pockets preferentially occur at interfaces between high density metal or troilite, and low density silicate phases, particularly plagioclase (Dodd and Jarosewich, 1979; Stoffler et al., 1991). At low degrees of shock, melt pockets are not interconnected at scales exceeding 2 mm. These melt pockets are recognised as irregularly shaped domains containing variable proportions of either (1) glass-like silicate material (cf. Stoffler et al., 1991; henceforth referred to as silicate glass) with spherical metal-only, metal–troilite or troilite-only inclusions (Fig. 1A), or (2) metal and/or troilite with numerous spherical inclusions of silicate glass (Fig. 1B). These represent two different liquid emulsions with distinct physical properties. To describe the composition of these emulsions we will refer to them, for example, as metal-dominated emulsions, meaning immiscible silicate melt globules contained within metal melt, or silicate-dominated emulsions, meaning the opposite.

The impact heating process responsible for this incipient melting was typically tightly spatially focused such that even in conjoined metal–troilite grains, the dense phase involved in melting was either (1) FeNi metal only (Fig. 1A and B), (2) troilite only (Fig. 1C), or (3) both metal and troilite, forming mixed metal–sulfide melts (Fig. 1D). Within some zoned metal grains there is variability in the way different metal compositions were incorporated within the silicate melt (Fig. 2). At shock Stages S5 and S6 there is more pervasive development of melt pockets throughout a given OC sample (Stoffler et al., 1991).

2.2. Glassy silicate veins and breccias

A separate melt formation mechanism can also be active along spatially focused fault planes that are thought to

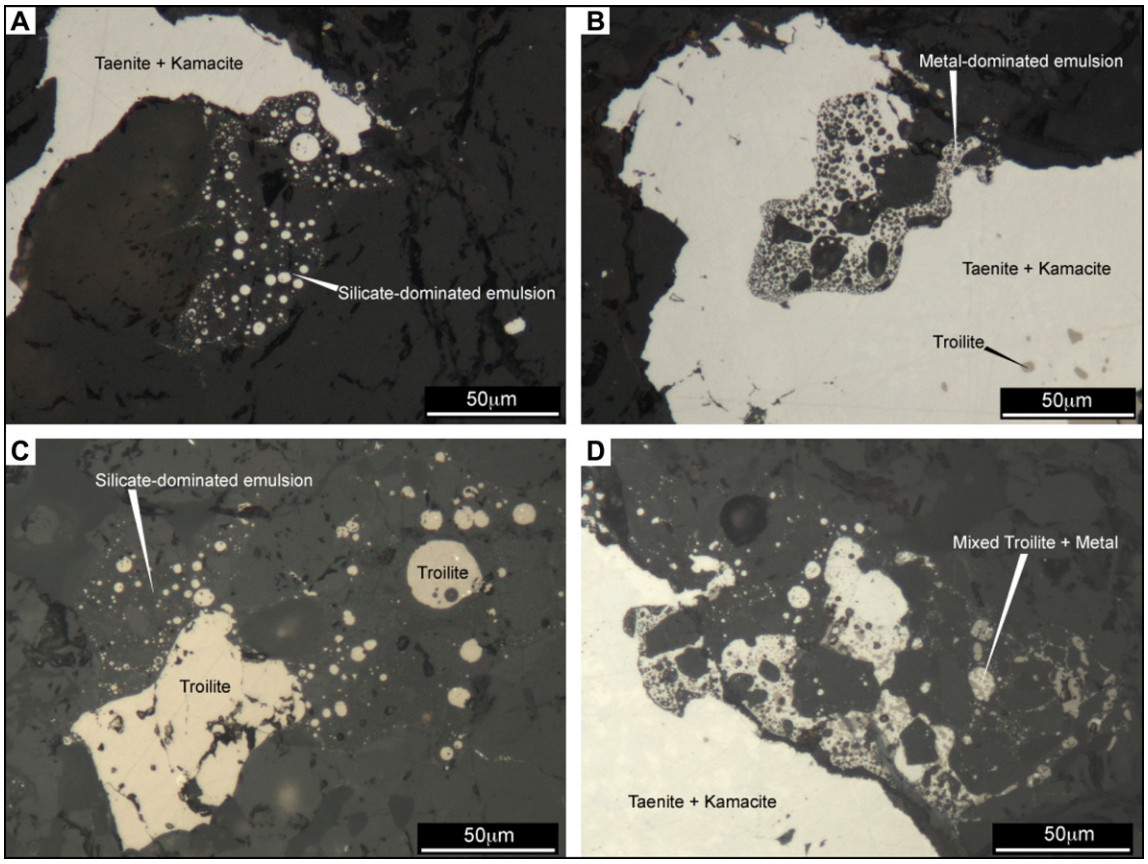

Fig. 1. Reflected light digital images of melt pockets preserved in NWA 869 an L4-6 ordinary chondrite polymict breccia. (A) Silicate-dominated emulsion developed at the contact between exsolved kamacite–taenite metal and olivine, with metal globules entrained in silicate glass. (B) Metal-dominated emulsion developed at the contact between exsolved kamacite–taenite and olivine. (C) Silicate dominated emulsion with troilite and only trace metal globules in silicate glass. (D) A more complex melt pocket with large irregular globules of metal–sulfide dominated emulsion entrained in silicate dominated emulsion. The metal/sulfide globules are metal-dominated in some parts and troilite-dominant in others. In A, B and D, disruption of the exsolved kamacite–taenite texture indicates that the impact responsible happened after considerable cooling from peak radiogenic metamorphism (see Reisner and Goldstein, 2003; Tomkins, 2009).

accommodate movement associated with crater formation (see Stoffler et al., 1991). Sub-millimetre to decimetre-long fault planes are observed in many meteorites, and these could conceivably exceed a kilometre within impact structures (much larger examples are observed on Earth where the energy released by impacts was greater; see Keil et al., 1997). Extreme strain rates on these fault planes cause fracturing, brecciation and frictional melting. This process promotes development of through-going melt veins, which are considered to be analogous to pseudotachylite veins in impact structures on Earth (cf. Stoffler et al., 1991; Melosh, 2005). Observations of OC meteorites show that the resulting melt veins are complex, containing primarily silicate-dominated emulsions that transition into metal–troilite veinlets (Fig. 3).

Glassy silicate melt veins vary considerably in width; most being <1 mm, although glassy vein networks >5 cm in width are observed in some OC meteorites (Fig. 4). Wider veins tend to be filled by silicate-dominated emulsion and are typically characterised by margins with numerous miniscule metal/troilite droplets and interiors with fewer large droplets (Fig. 3A). In some wider melt veins, one or both margins instead display linked metal–troilite veins (Fig. 3B; i.e., the micro-droplets have linked together). In other wider veins, curved droplet trails indicate the direction of melt migration (Fig. 3C).

2.3. Small-scale metal–troilite veins and breccias

Other glassy silicate melt veins show domains with boudinage or breccia texture, with mixed metal–troilite filling the boudin necks or breccia matrix (Fig. 5A–C; boudinage is an extensional structural feature whereby a more competent layer is pulled apart lengthwise creating sausage-like boudins separated by thinning or breakages at boudin necks). The metal to troilite ratio in these fillings varies considerably, some being dominantly metal. Rounded clasts of unmelted chondrite material caught up in the glassy silicate veins (Fig. 4) typically contain coarse metal/troilite-filled extension fractures developed approximately perpendicular to the length of the glassy vein and numerous fine troilite-dominant veinlets. In many cases these breccia clasts are partially surrounded by a thin metal–troilite vein, which tend to be thicker in what are interpreted to be pressure

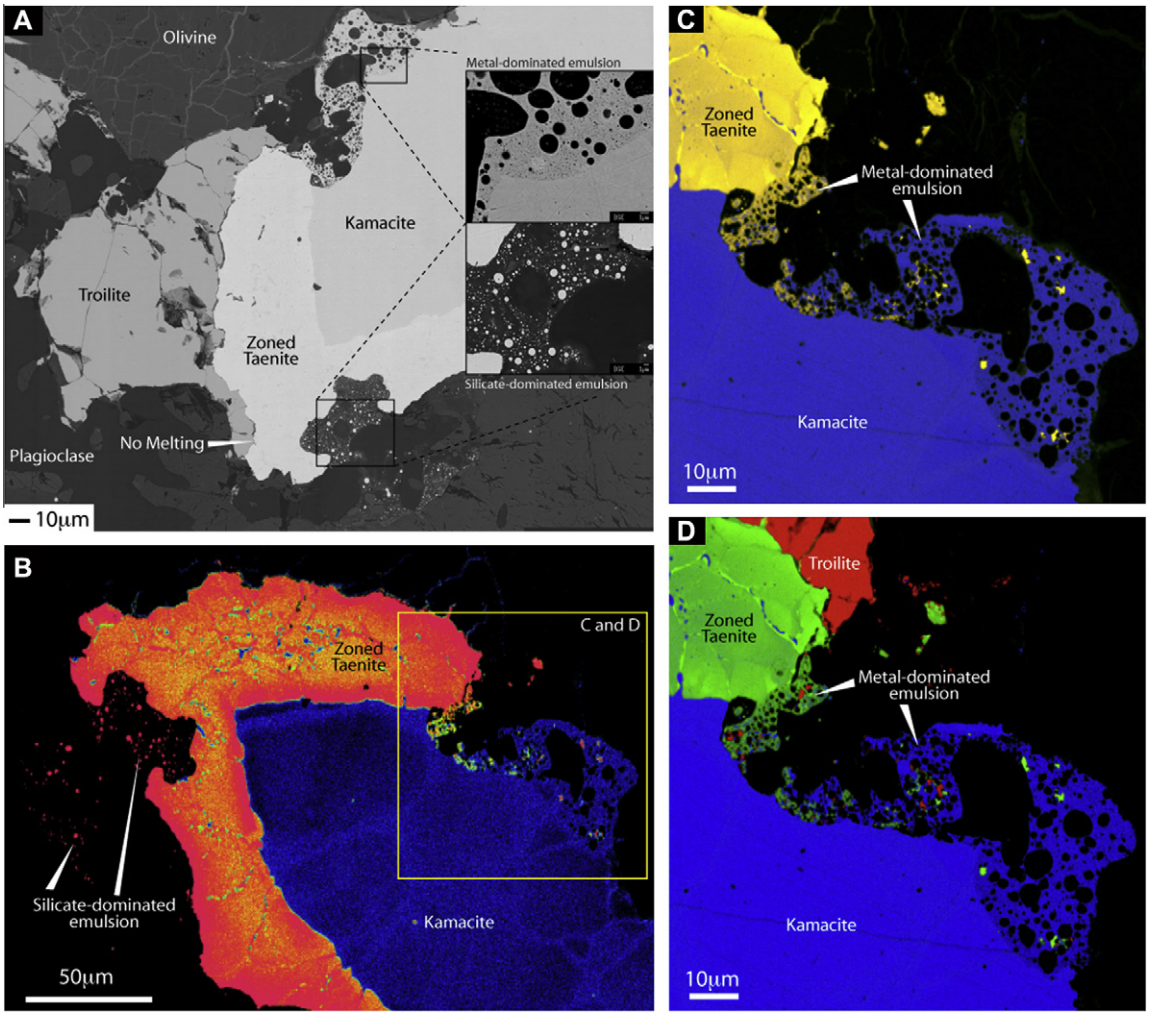

Fig. 2. Heterogeneity of melt pocket compositions around a composite metal–troilite grain in NWA 869. (A) Back-scattered electron images (generated on a JEOL 7001F FEG-SEM) of two different melt emulsions generated at metal–plagioclase interfaces. The metal component is comprised of a kamacite domain and a zoned taenite domain, which would have formed during cooling after peak radiogenic metamorphism (see Reisner and Goldstein, 2003; Tomkins, 2009). In the upper region a metal-dominated emulsion contains numerous spherical silicate globules, and a silicate-dominated emulsion developed in the lower area has numerous spherical metal globules. (B) Element map (generated on a JEOL 8500F CL HyperProbe operating at 10 kV, 50 nA, dwell time 30 ms, pixel size = 200 nm) showing the variability in Ni/Fe ratio in the metal domains in A (yellow to red = increasing Ni/Fe = taenite to tetrataenite, blue = low Ni/Fe = kamacite). It can be seen that the Ni content of metal in the two melt emulsions is significantly different and reflects the metal composition adjacent to each melt pocket. (C) Close-up Ni–Fe element map (collected at 7 kV, 40 nA, dwell time 60 ms, pixel size = 100 nm) of taenite (yellow; brighter = higher Ni) and kamacite (blue) distribution in the metal-dominated emulsion. D. Element map for Ni, Fe and S (same probe conditions as C; green, increasing brightness = increasing Ni in taenite–tetrataenite, blue = high Fe kamacite, red = high S = troilite). In C and D, significant compositional heterogeneity is evident in the melt domain, varying as a function of mixing between melt from the zoned taenite domain and that from the kamacite domain. The melt domain is not enriched in Ni relative to the unmelted metal residue. A small proportion of troilite at the edge of this domain has melted, but the melt is not remotely near the FeNi–FeS eutectic composition of ~85% FeS.

shadow regions developed perpendicular to the melt flow direction. Where linked metal–troilite veins occur adjacent to, or sometimes within a silicate glass vein, fault relay structures are in some cases developed that link between nearby metal–troilite veins (Fig. 6A and B; fault relay structures are cross-cutting failure planes that link approximately parallel faults; they develop to equilibrate movement across the parallel fault system). These boudinage and breccia textures, extension fractures and fault relay structures are considered to be transitional to metal–troilite vein networks that are not clearly connected to the glassy silicate veins.

2.4. Troilite-dominated micro-veins and micro-breccias

Troilite-dominated sub-micron vein or micro-breccia networks are typically observed adjacent to thicker metal–troilite veins (Fig. 6). The breccias typically contain angular

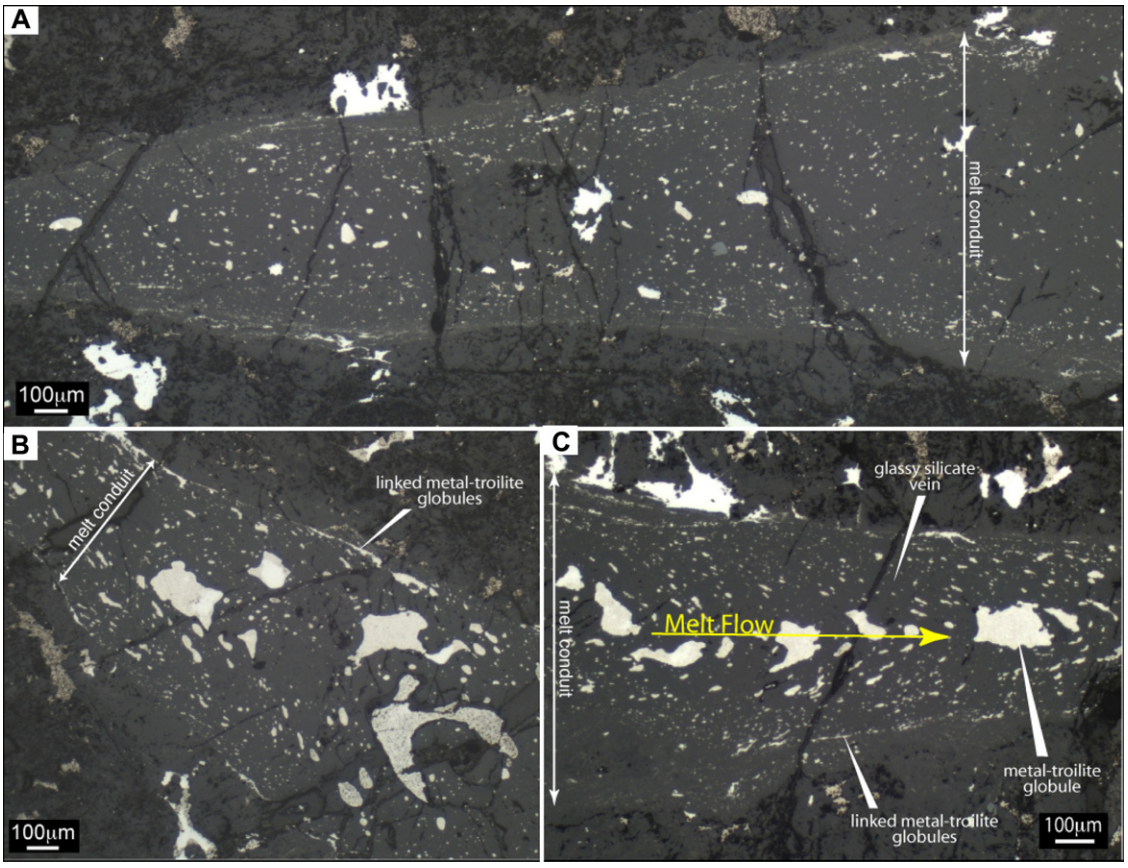

Fig. 3. Glassy silicate veins, comprised of silicate-dominated emulsion, in the Chergach meteorite (an H5 ordinary chondrite; these are reflected light digital images of the dark domains in Fig. 4A, though from a different sample). All of the globules in the silicate-dominated emulsions are comprised of quench-textured mixed metal–troilite. (A) An example of the globule size distribution across a vein, with coarse metal–troilite globules at the centre, grading to fine droplets at the margins. (B) and (C) Examples of linked fine metal–troilite droplets at vein margins (better developed in B) and curved droplet trails indicate silicate melt flow direction (better developed in C).

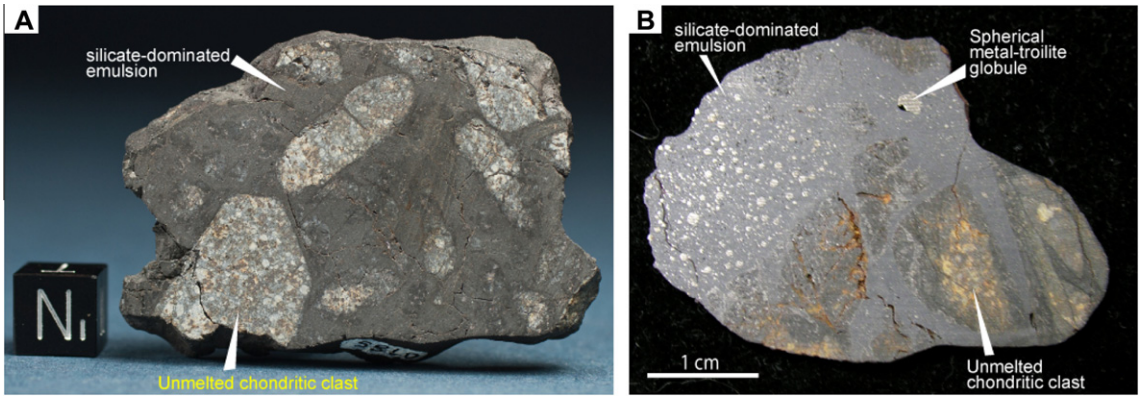

Fig. 4. Examples of the impact melt breccias preserved in the Chergach (A; the scale cube is 1 cm) and Gao–Guenie (B) meteorites (Gao–Guenie is an H5 ordinary chondrite). The dark domains are the glassy silicate melt veins shown in Fig. 3. Note the well-rounded morphology of the unmelted silicate clasts in both examples. The Gao–Guenie example has been angled to highlight the metal distribution, which shows coarse spherical metal–troilite globules at the centre of the largest melt vein. The photograph of Chergach was provided by Dr. Svend Buhl of Meteorite Recon.

silicate fragments separated by films of troilite (Fig. 6C; narrowest measured are 20 nm wide), and sparse FeNi metal tends to occur at junctions between fragments (Fig. 6D). Within these systems, metal tends to be concentrated in thicker veins, so the process responsible for troilite microbreccia development caused sulfide to separate from metal.

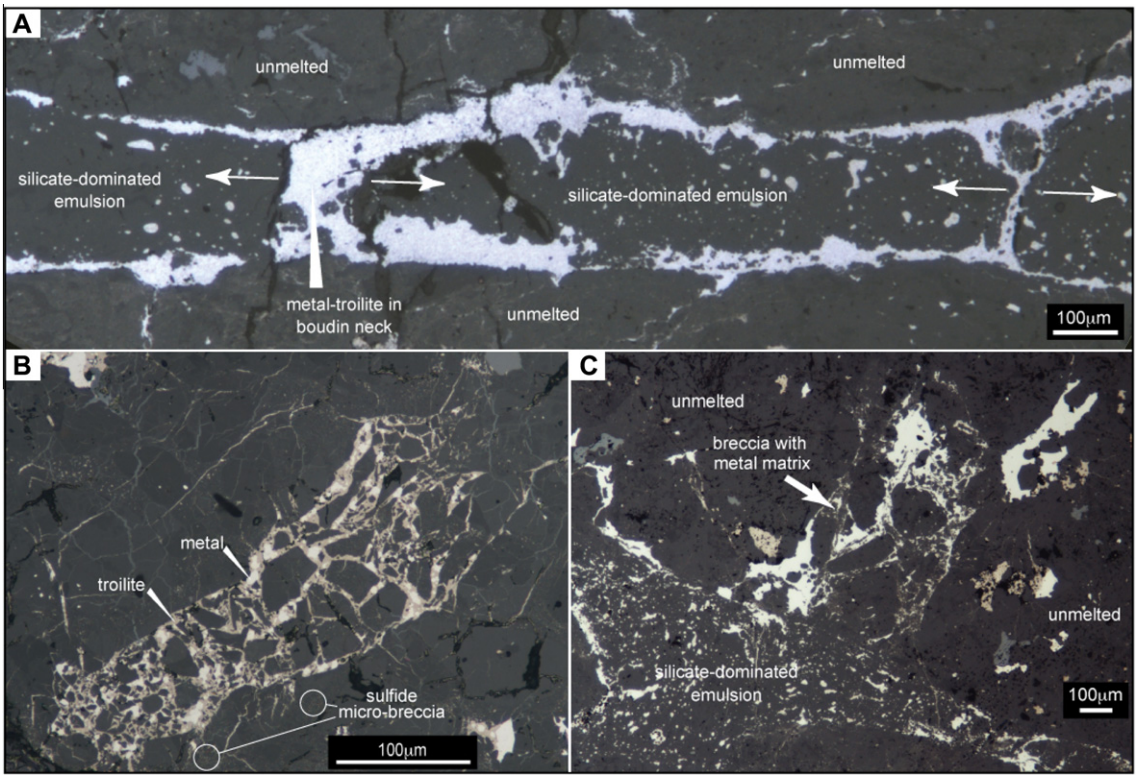

Fig. 5. Examples of localised dilational settings developed within the frictional melt vein systems preserved in the Chergach (A and C) and La Criolla (B) meteorites (La Criolla is a L6 ordinary chondrite). (A) A silicate dominated melt emulsion with metal–troilite veins on both margins that has been boudiaged. Dilational sites are developed at boudin necks, resulting in metal–sulfide melt infiltration and accumulation. (B) A troilite–metal cemented breccia with jig-saw fitting largely unmelted silicate clasts. Poorly resolved at this scale are patches of troilite-dominated micro-breccias adjacent to the main breccia (more are present than outlines; see example in Fig. 6). (C) A metal-cemented breccia adjacent to one of the glassy silicate veins shown in Fig. 3. All are reflected light digital images.

2.5. Meso-scale metal veins and nodules in samples largely lacking silicate glass

Other meteorites lack the glassy silicate veins, but instead contain metal-dominant veins and sometimes troilite-only micro-veins. These metal veins can be many centimetres long and typically 5 μm to 3 mm wide, and in samples with multiple veins these are usually oriented parallel to one another or at conjugate angles (Fig. 7), or can show curvilinear orientations. Some of these veined samples also contain incipient silicate melt pockets, although others do not. In some of these samples, large isolated metal globules (some >5 mm) are found, which may have been connected to the vein system. Metal veins and nodules have been studied previously by Widom et al. (1986), Kong et al. (1998), Rubin (1999) and Rubin (2002) who found that the metal is typically depleted in the most refractory siderophile elements (PGE) and Cu, but are not depleted in Ni, Co, W, Mo, Au, As and Sb relative to fine-grained metal. These authors are in general agreement that metal nodules form through impact-related processes, although the exact mechanism is not well constrained. Current theory suggests that they formed through vapour deposition after impact vapourisation (Widom et al., 1986; Rubin, 1999), although no physical evidence or thermodynamic argument has been presented to show that this was the case.

2.6. Large-scale metal veins and breccias

In rare impact affected OC meteorites these larger metal veins can be several centimetres thick, and even form a breccia matrix. In the H6 ordinary chondrite, Portales Valley, the vein and breccia matrix metal is sulfide-depleted (Fig. 8A), whereas the angular, jig-saw-fitting breccia clasts are sulfide-enriched and metal-depleted (Kring et al., 1999; Rubin et al., 2001; Ruzicka et al., 2005). The coarse metal veins in this meteorite have Widmanstatten texture, which evolves through slow cooling, indicating that they were insulated deep within the H chondrite parent body (Rubin et al., 2001). It has been suggested that pre-shock temperatures for Portales Valley were high (age data are consistent with an early impact event) and that this may have facilitated melting and melt segregation (Ruzicka et al., 2005), which again implies that the brecciation event took place deep within the H chondrite parent body. These authors used equilibrium-based modelling to suggest that liquid and solid metal were mobilised in a shearing-related process, although the mechanism by which deformation caused

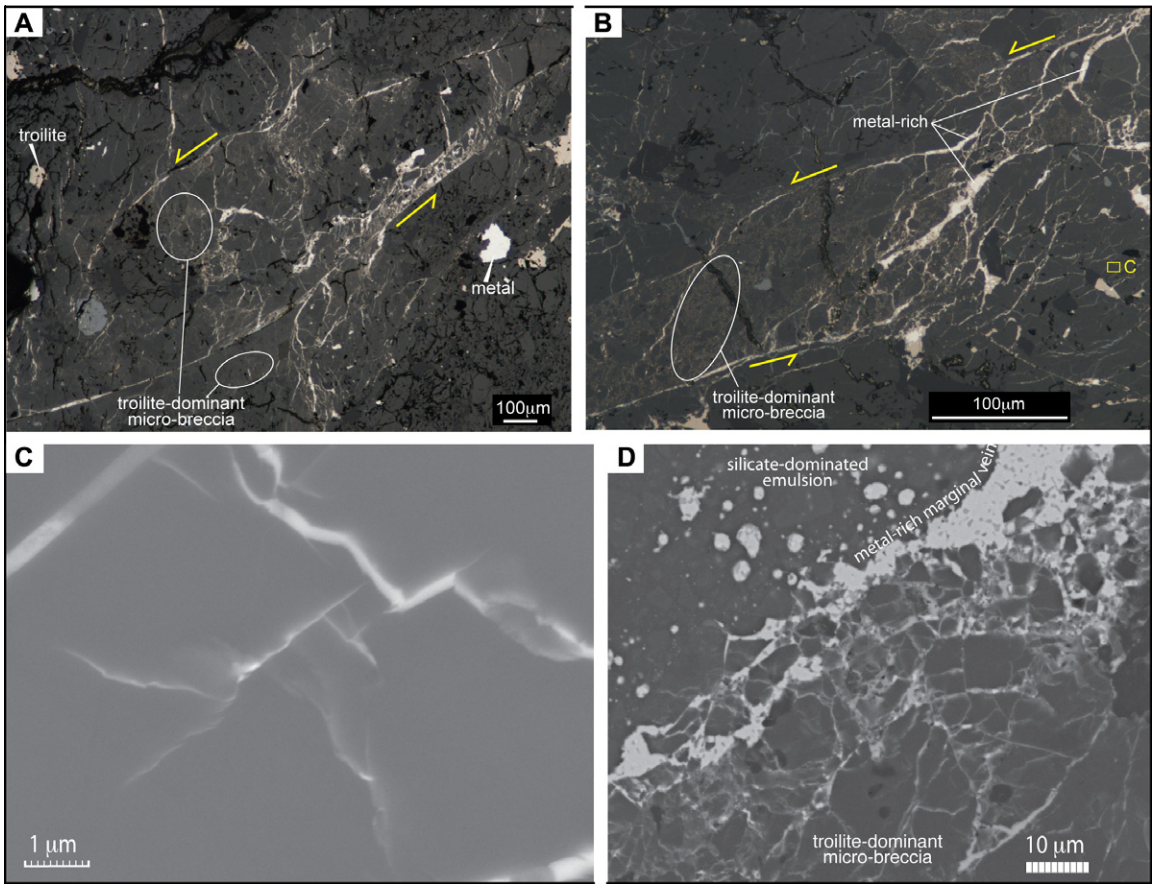

Fig. 6. Examples of structures that facilitate metal/sulfide melt migration and accumulation; developed in the La Criolla (A–C) and Chergach (D) meteorites. In A and B troilite metal–troilite filled vein networks are developed within interpreted fault relay structures. The interpretation is based on our previous experience, and that of many others, in studying hydrothermal quartz veins in orogenic gold deposits, which form during compressional deformation through hydraulic fracture-driven fluid infiltration (e.g., see Cox, 2005, and Fig. 10 in Miller and Wilson, 2005). In C is a BSE image showing a close-up from the small box at the middle-right of B, highlighting the fine structure of the troilite-coated fractures (generated on a JEOL 7001F FEG-SEM with 5 nm resolution). (D) An example of the troilite-dominant micro-breccia, which is developed marginal to a metal-dominated vein, which is itself developed at the margin of one of the silicate-dominated emulsion veins shown in Fig. 3. Note that at this resolution many of the troilite films between angular silicate fragments are <100 nm thick, and that sparse metal (brighter) tends to occur at junctions between silicate clasts; metal is also more abundant closer to the metal-rich vein.

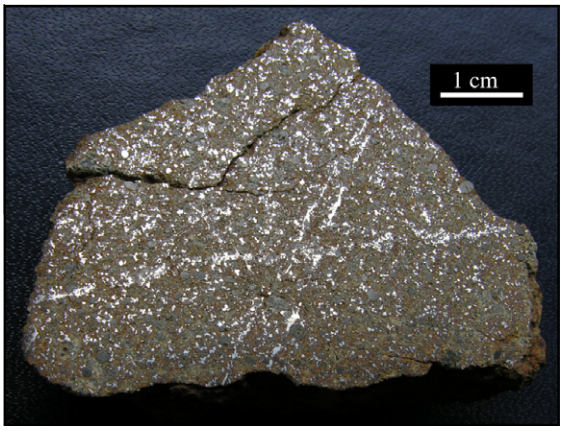

Fig. 7. Coarse parallel and conjugate metal-only veins in the Windimurra H4/5 ordinary chondrite. Dark spherical chondrules can be seen sitting in a highly porous matrix. There are no silicate-bearing melt veins in this sample.

metal mobilisation and separation of sulfide from metal was not discussed.

2.7. Nonmagmatic iron meteorites

As noted by others (see Ruzicka et al., 2005), the breccia textures in Portales Valley are reminiscent of the textures of some nonmagmatic iron meteorites (types IAB and IIE). These meteorites comprise 23% of grouped iron meteorites and, with a large number of sub-groups (Wasson and Kallemeyn, 2002), thus represent a widespread geochemical process of metal segregation that was taking place early in the evolution of the solar system. In contrast to the magmatic iron meteorites, the trace element compositional trends of nonmagmatic iron meteorites cannot be explained by simple fractional crystallisation (Scott, 1972; Scott and Wasson, 1975; Haack and McCoy, 2003). It is generally agreed that these meteorites formed by partial melting then migration and accumulation of metallic melt during impact

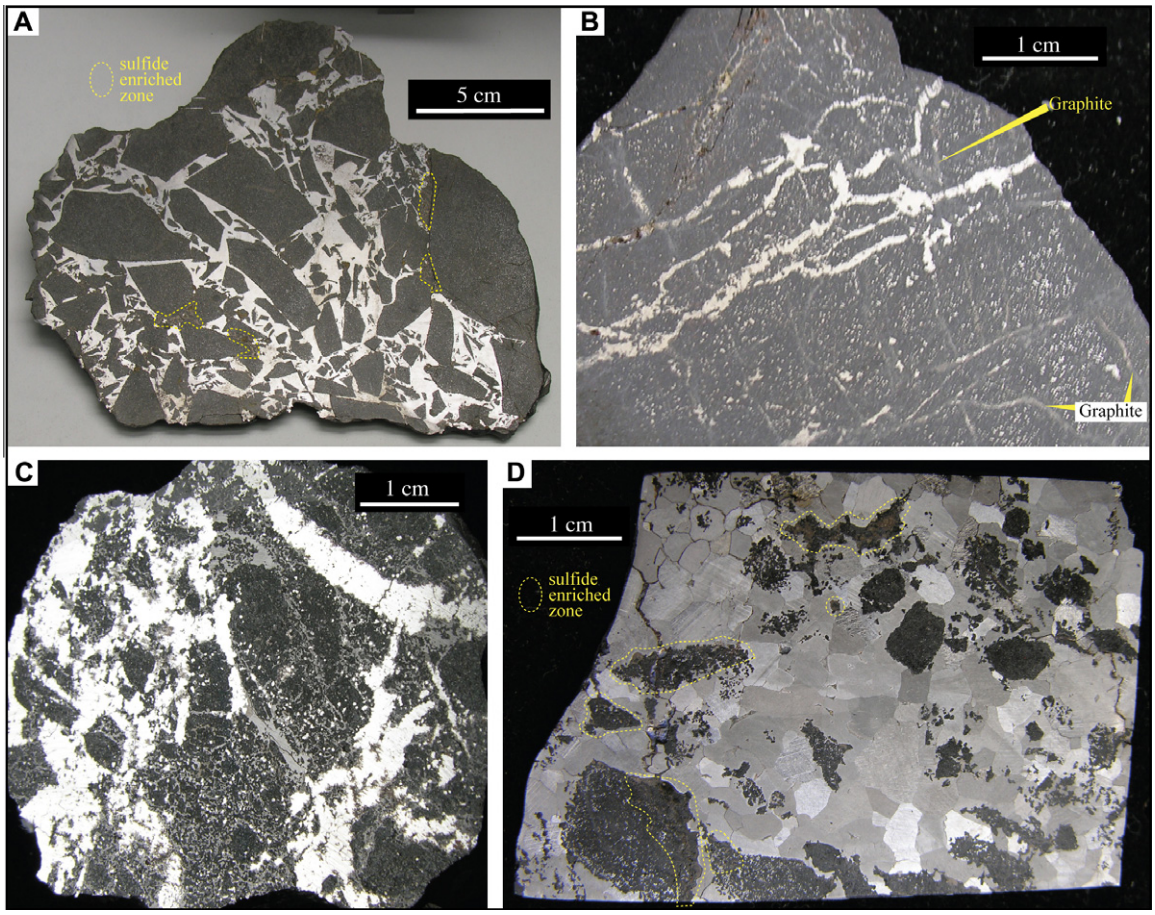

Fig. 8. Large-scale metal cemented breccias and veins. (A) The Portales Valley meteorite with angular clasts of H6 ordinary chondrite material within an FeNi metal matrix. Some highly sulfide-enriched domains amongst silicate material are outlined with yellow dashed lines. (B) and (C) Silicate-rich samples from the Campo del Cielo suite of IAB (nonmagmatic) iron meteorites (total mass >100 tonnes). Metal veins (bright) can be seen transecting the silicate material (dark grey), together with abundant graphite (lighter grey). Metal veins in these samples typically have euhedral hexagonal graphite crystals in the metal, and margins that are rimmed by graphite. (D) Abundant chondritic clasts in NWA 5549, another IAB (nonmagmatic) iron meteorite. Some of the chondritic clasts have domains that are sulfide enriched (dashed yellow outlines). (For interpretation of the references to colour in this figure legend, the reader is referred to the web version of this article.)

events (see Haack and McCoy, 2003; Ruzicka and Hutson, 2010), although again, the mechanism responsible for melt migration is poorly defined. The $\varepsilon^{182}W$ ages of nonmagmatic iron meteorites are slightly younger than magmatic irons (Qin et al., 2008; Carlson and Boyet, 2009), implying that the formation of both groups was influenced by radiogenic heating.

We have examined two silicate-bearing IAB iron meteorites as part of this study: Campo del Cielo and NWA 5549. Both of these meteorites contain angular chondritic clasts, and rare samples of Campo del Cielo consist dominantly of silicate material with metal + graphite veins (Fig. 8). As with Portales Valley, the metal is sulfide-depleted and the silicate domains are comparatively troilite-rich in both of these samples, with some clasts in NWA 5549 being highly troilite-enriched (Fig. 8D). The silicate clasts have embayed and occasionally indistinct margins, like some of those in Portales Valley (Ruzicka et al., 2005), and the troilite in the silicate domains dominantly consists of an interconnected network amongst silicate grains rather than veinlets. Others have described similar chondritic fragments amongst metal in more comprehensive studies on nonmagmatic iron meteorites (e.g., Casanova et al., 1995; Benedix et al., 2000; Bogard et al., 2000; Ruzicka and Hutson, 2010).

Models for the genesis of nonmagmatic iron meteorites include gravitational segregation and ponding of FeNi melt in response to impact heating (Wasson et al., 1980; Wasson and Wang, 1986; Olsen et al., 1994; Choi et al., 1995; Wasson and Kallemeyn, 2002), incipient parent-body melting during endogenic heating (McCoy et al., 1993; Bogard et al., 2000), or a hybrid combination of these where impacts into an already hot parent body drove mixing between metal and silicate (see references in Ruzicka and Hutson, 2010). A key feature of the nonmagmatic iron meteorites that any model must be able to explain is their siderophile element signatures, which imply limited trace element partitioning between solid metal and melt and thus possibly segregation of metallic melt from a partially molten source (see Wasson and Kallemeyn, 2002). Other than

assuming that separation of metal from silicate was driven by gravitational segregation (e.g., ponding), none of the existing models examine in detail the mechanisms responsible for migration of FeNi melt.

3. THE DRIVING MECHANISMS OF MELT MIGRATION

In the following discussion, and in subsequent sections, we consider impact melting and melt migration from the perspective of three separate stages: Stage 1 – associated with the impact pressure wave (discussed in Section 4), Stage 2 – associated with rock movement and deformation in response to crater formation, and Stage 3 – associated with cooling after cessation of movement.

3.1. Pressure gradients in deforming environments

The driver for migration of any fluid is a pressure gradient. Understanding causes of melt migration in asteroids and planetesimals is therefore about understanding how pressure gradients are generated. Fluids migrate through porous rocks (e.g., the fracture networks shown in Fig. 6 represent porosity, and a permeable network while melt is present) towards regions of comparatively low pressure, according to Darcy's Law:

$$Q/At = (k/\mu)(dP/L) \quad (1)$$

where Q/At is the fluid flux (fluid volume, Q, across cross-sectional area, A, per unit time, t; ms^{-1}), k is the permeability of the rock (m^2), μ is the viscosity of the fluid (Pa s), dP/L is the pressure gradient (Pa m^{-1}).

During deformation associated with an impact event, regions of comparatively high and low pressure are developed as some regions are compressed and other regions either remain the same, or actively dilate. In deforming rocks, large differences in pressure are typically focused on or in the vicinity of faults and fractures (Cox, 2005). Impact craters develop these zones of dilation and compression at every range in scale from microfractures up to large fault systems. The process of fracture dilation induces a localised pressure drop within the fracture, or fracture zone, which promotes inward migration of mobile components. Zones of compression create regions of higher pressure that mobile phases move away from, through whatever permeable paths exist within the rock mass. In a deforming environment with a gravitational gradient and an existing fracture network Darcy's Law becomes:

$$Q/At = (k/\mu)[\partial(P - \rho gh)/\partial x] \quad (2)$$

where $[\partial(P - \rho gh)/\partial x]$ is the hydraulic gradient for fluid flow via fractures along path x (Manning and Ingebritsen, 1999).

However, fluids also create permeability in deforming systems through hydraulic fracturing (e.g., Barnhoorn et al., 2010). Increased pressure in regions of compression on a fluid-filled fracture can cause the fracture tip to rupture where the fluid pressure exceeds the fracture toughness of the rock. This hydraulic fracture propagation process enhances the existing fracture-controlled permeability of the system and thus facilitates migration of metal/sulfide melt towards lower pressure domains.

The distance that can be covered during melt migration through a given fracture is a function of the period of time that the melt remains liquid (see Section 4 for discussion of melt lifetimes), the period of time that the pressure differential exists, the square of the fracture width, and inversely proportional to the viscosity of the melt (Poiselle's Law). For a given localised instance of melting all of these factors will be the same, except for the viscosities of the different melts. Thus, for a given pressure gradient, low viscosity metal melt ($\eta = 0.004$ Pa s^{-1}; Shimoji and Itami, 1986) will migrate ~50 times faster than melted troilite ($\eta = 0.2$ Pa s^{-1}; Dobson et al., 2000), ~2500 times faster than basaltic melt ($\eta \approx 10$ Pa s^{-1} at 1250 °C; Villeneuve et al., 2008), and $\sim 8 \times 10^9$ times faster than liquid plagioclase ($\eta \approx 3.2 \times 10^7$ Pa s^{-1} for An_{10} chondritic plagioclase at 1250 °C; Hummel and Arndt, 1985). Composite FeNi–FeS melts have viscosities comparable to Fe and FeS liquids, so metal, sulfide and metal–sulfide melts would migrate significantly further than silicate melt along any short-lived pressure gradient generated through impact. In addition, pressure gradients, and thus fluid flux, are proportional to the deformation rate, so during high energy impact events the pressure differentials generated are likely to be very high, thus maximising $\partial P/\partial x$ in Eq. (2). Therefore, on asteroids and planetesimals, where low gravity minimises ρgh, the influence of gravitational gradient on fluid flow in Eq. (2) becomes negligible, and fluid flow is controlled dominantly by deformation-driven pressure gradients.

3.2. Progressive metal melt extraction across a range of scales (Stage 2)

Once friction-generated silicate-dominated melt emulsion networks form (e.g., Fig. 4), melt migration is controlled by the physical characteristics of silicate melt, as evidenced by the curved metal–troilite droplet trails in glassy silicate veins (Fig. 3). The marginal metal–troilite veinlets associated with these probably evolved by viscosity segregation (Fig. 9), where the lower viscosity of the metal–sulfide melt caused it to migrate to the wall of the melt conduit, minimising shear stress and maximising the energy efficiency of the system (see Carrigan and Eichelberger, 1990).

Before the micro-droplets at the vein margins become linked, the velocity of melt migration is highest at the centre of the conduit, and progressively lower towards the margins, defining a parabolic velocity profile (Fig. 9A). However, once the metal–sulfide droplets migrate to the margins and link to form the marginal veins, they will dominate subsequent melt migration velocity because the much lower viscosity of metal–sulfide melt allows it to respond more rapidly to pressure differentials. Thus lubricated, silicate melt-filled conduits become piston-like and migration becomes more rapid, with nearly all of the strain taken up by the marginal metal/sulfide melt (Fig. 9B). Where this piston-like behaviour departs from ideality due to structural heterogeneities in three dimensions, the silicate-dominated component is forced to deform rapidly and its glass

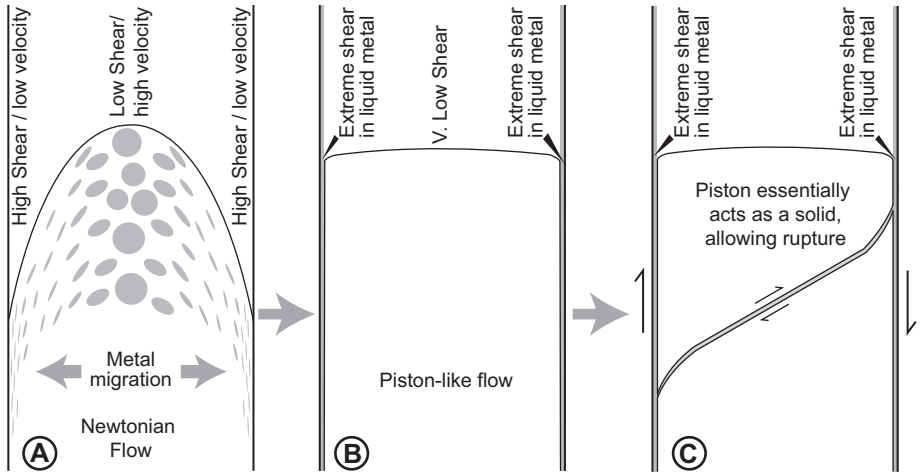

Fig. 9. Schematic representation of the physical response of silicate-dominated emulsion-filled veins to rapid melt migration. Based on the concepts of Carrigan and Eichelberger (1990).

transition can be exceeded (Fig. 9C), allowing it to fracture and then be boudinaged (e.g., Fig. 5A) or brecciated (e.g., Fig. 5B and C; extension at the narrower boudin necks creates pressure gradients that cause mobile liquid phases migrate towards these sites). Solid clasts of silicate material between melt veins are also placed under stress during this process and numerous fractures are observed in these.

Once the metal–sulfide melt has become independent of the silicate melt, evidence shows that it is able to migrate into unmelted silicate domains (Fig. 6). The migration pathways may be a distributed fracture network (see Barnhoorn et al., 2010), which may be somewhat permeable while deformation is active, and are likely to be enhanced by hydraulic fracturing in areas where high fluid pressure can be generated within fractures. In these settings, we have observed fault relay structures that developed between adjacent metal/sulfide melt-lubricated faults (Fig. 6A and B). In each of the settings shown in Figs. 5 and 6, localised structural dilatancies developed as fracture margins pulled apart, which allowed formation of wider, more permeable and thus longer-lived metal–sulfide-filled vein systems. Vein structures and fractures that form in deforming systems tend to be somewhat fractal (Johnston and McCaffrey, 1996; Bonnet et al., 2001; Nortje et al., 2006; Fagereng, 2011), where structural features developed at the small scale are to some extent replicated at the larger scale. In meteorites, we can see that impact-induced deformation created linked networks of metal–sulfide melt at the micro- to meso-scale, increasing the permeability of the system, and allowing more rapid (see Rushmer and Petford, 2011) and larger scale migration from zones of overall compression to nearby zones where deformation was largely dilational. We suggest that this pattern would be to some extent mimicked at the larger scale that cannot be sampled in entirety by meteorites (represented schematically in Fig. 10).

In some meteorites (Figs. 7 and 8A), a dominantly dilational setting is inferred from the observation of jagged margins to metal-only veins and enlarged nodules (some have minor sulfide) in samples that have not undergone significant recrystallisation, as evidenced by the presence of well-preserved chondrules. These metal-only veins can be several centimetres long, and penetrate chondrite material that is not metal-depleted, implying that metal migrated into these fractures from elsewhere (i.e., there appears to have been volume increase). In these samples, there may be little or no evidence for melting of silicate phases, again implying that the vein- and nodule-hosted metal is externally derived. Vapour deposition of the metal in these veins and nodules, as suggested by Widom et al. (1986) and Rubin (1999), is considered highly unlikely because OC meteorites typically have considerable porosity (Britt and Consolmagno, 2003; Sasso et al., 2009), and there can thus be little structural control on vapour localisation. The conjugate nature of some of these vein sets (Fig. 7) is clearly deformation-induced, and we consider these structures to be transitional to larger-scale systems (as represented by Fig. 10C).

Because melt migration during impact events is controlled by deformation-induced pressure differentials with minimal influence of gravity (see discussion concerning Eq. (2)), metal melt can entrain chondritic fragments without their being excluded by buoyancy (e.g., Fig. 5B). In contrast, melt segregation that is driven by gravity would inherently exclude chondritic clasts due the large difference in density between metal and silicate chondrite material that drives melt percolation. The observation of angular chondritic clasts enveloped in a metal matrix in Portales Valley thus suggests that deformation-induced metal melt migration was responsible for formation of this texture. The existence of angular chondritic clasts in many of the IAB and IIE nonmagmatic iron meteorites has been a conundrum for many years because of the recognised buoyancy issue (see Ruzicka and Hutson, 2010). We suggest that these chondritic clasts imply that nonmagmatic irons also formed by deformation-induced melt migration. Thus, Portales Valley and the nonmagmatic iron meteorites are considered to be representatives of the larger scale end of the metal-melt accumulation process (Fig. 10D and E respectively).

To form a large accumulation of metal liquid, metal must be extracted from a certain volume and focused into a structural feature during a short-lived impact-induced

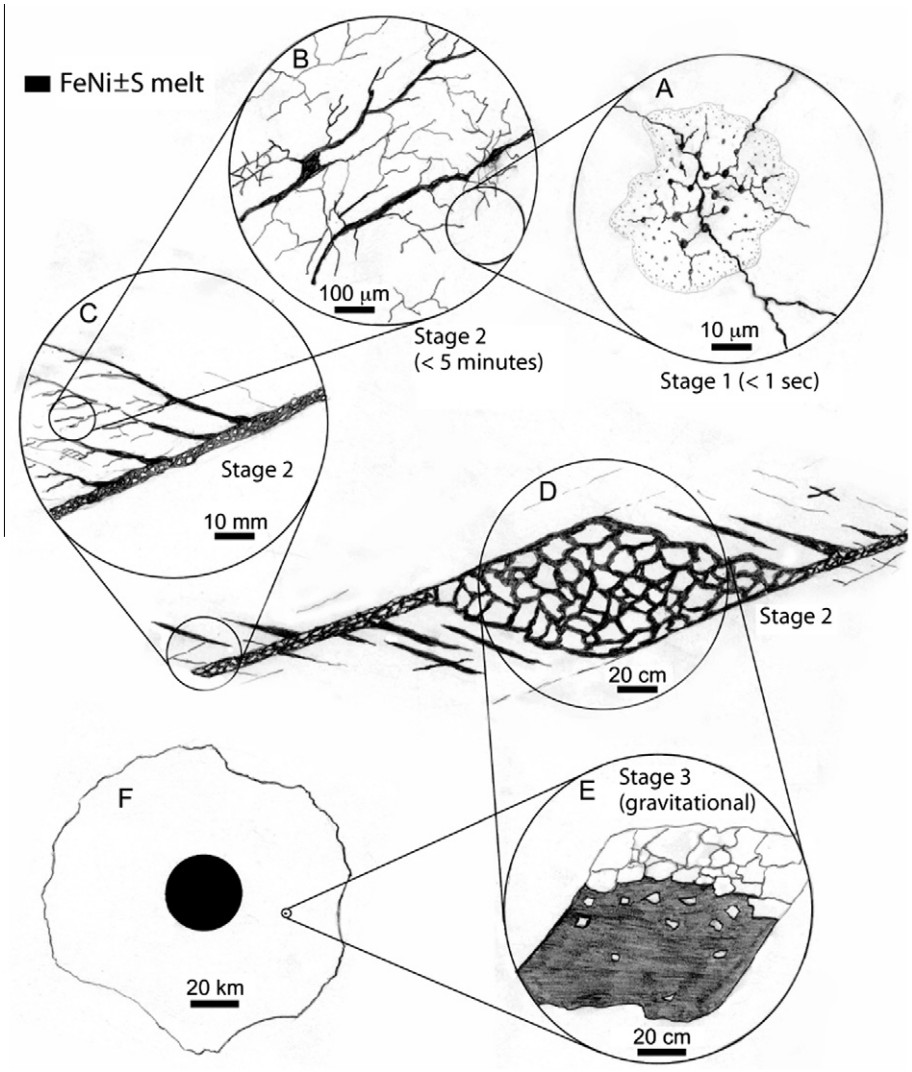

Fig. 10. Schematic representation of the different scales and stages in the impact-driven segregation of large Fe–Ni–S melt accumulations. (A) is equivalent to Figs. 1 and 2. (B) is equivalent to Figs. 3, 5 and 6. (C) is equivalent to Fig. 7. (D) is equivalent to Fig. 8A. (E) is equivalent to Fig. 8D and other nonmagmatic iron meteorites. (F) is aimed at indicating the position of a given accumulation within a planetesimal that continues to grow after its formation, and then eventually undergo silicate melting.

deformation event. In Portales Valley, Rubin et al. (2001) found that metal-depleted silicate clasts had lost 30–80% of their metal. A typical H chondrite contains ~10 vol.% metal, so at an extraction efficiency of 50%, a 1 m^3 volume of liquid metal would need to be sourced from 20 m^3 of chondritic material within the few minutes duration of an impact driven deformation event. Eq. (2) indicates that the rate of liquid metal extraction will vary as a function of the cross-sectional area through which it is being extracted. So as an example, given a 5 × 2 m fault plane bordered by a 1 m thick volume of fractured chondritic material on either side of the fault (so 20 m^3 of rock volume and 20 m^2 of fault plane surface area since there are two sides), with a permeability of 9.87×10^{-11} m^2 (appropriate for highly fractured rock), extraction of this volume of low viscosity metal in the time available would require a hydraulic pressure gradient of 1.44×10^5 Pa m^{-1} for migration of 1 m^3 liquid metal in 2 min. In other words, the pressure differential between chondrite at 1 m away from the fault and chondrite at the fault plane needs to be only 1.44 bar, and this changes to 2.89 bar if the pressure differential is maintained for 1 min (17.32 bar for 10 s). These pressure gradients are expected to be achievable during high energy impact events, although more complex modelling is needed to show that this is indeed so. More important effects are likely to be the extent of melting of the metal and the permeability of the chondritic material. Impact fractured rocks can be highly permeable, and become more so with hydraulic fracturing. Extensive metal melting would also generate silicate melt, and this would create complexity in the permeability of the system.

3.3. Separation of sulfide from metal (Stage 3)

A mechanism is required to explain the observed troilite enrichment in silicate material that almost invariably occurs

adjacent to zones of metal–sulfide melt accumulation. In Fig. 6D it can be seen that thicker veins tend to be relatively metal-rich, linked with numerous troilite-dominated submicron veinlets and micro-breccias developed in silicate minerals, indicating that sulfide-rich melt separated from metal to migrate into lateral fracture networks. This order of migration is preferred (rather than sulfide-dominated microfractures feeding into metal-rich melt accumulations) because the eutectic in the Fe–FeS system is at 85% FeS, so melts should fractionate towards sulfide-rich rather than metal-rich compositions.

It has been suggested that the troilite-enriched nature of chondritic clasts in Portales Valley formed when S_2 vapour was reintroduced along fractures and reacted with remaining metal to form troilite (Rubin et al., 2001). Troilite should partially devolatilise to Fe metal + S vapour in response to impact heating (see Lauretta et al., 1997; Tomkins, 2009). For this mechanism to work, Fe would be needed from the silicate minerals to form troilite, and since our microprobe work found no evidence of Fe-depleted vein margins, and some troilite-filled fractures occur in Fe-free plagioclase, we suggest that a S_2 vapour alone could not be responsible for the troilite-dominated veinlets and micro-breccias observed in this study. Rubin et al. (2001) also suggested that sulfide-rich melt infiltrated along fractures, migrating away from the metal veins, and Ruzicka et al. (2005) agreed, although neither study suggested a mechanism that would drive this melt migration. The hydraulic fracturing process drives vein and breccia formation, but this does not provide a completely satisfactory mechanism for separating sulfide from metal, particularly at larger scales.

Instead, we suggest the following. As metal–sulfide melt cooled and crystallised in larger fractures, probably after cessation of deformation, it evolved towards the FeNi–FeS eutectic. In cases where the liquid metal contained a small proportion of carbon, crystallisation of γFeNi would drive the liquid composition towards exsolution of immiscible iron carbide and iron sulfide liquids (see Fig. 4 in Corgne et al., 2008). Sulfide liquid is known to wet olivine (Gaetani and Grove, 1999; Barnes et al., 2008), whereas liquid Fe is known to be non-wetting against olivine (Minarik et al., 1996), although the wetting properties of sulfide-rich FeNi melts are not known. We suggest that as metal–sulfide melt fractionates and becomes sulfide-dominant its wetting properties against silicate material switch from being non-wetting to wetting, causing its dispersive adhesion properties (where one material is attracted and adheres to another via van der Waals forces; see Lee, 1991) with respect to the silicate material to switch from being repulsive to attractive. Such a switch would cause narrow fractures and grain boundaries in and between silicate minerals to start acting as capillary tubes for sulfide-dominant melt, drawing it away from crystallised metal (Fig. 11). In this case, the pressure differential driving melt migration is capillary pressure, and its magnitude increases with decreasing fracture width, so the finest fractures are the most effective at drawing in sulfide. It may be that some S_2 vapour is able to migrate into fractures and along grain boundaries together with sulfide-dominated melt, and in this case, reaction with small amounts of crystallising metal to form new troilite would further increase the FeS/FeNi ratio therein.

This tendency of sulfide to adhere to and infiltrate silicate material appears to exist at all scales where metal–sulfide melt coexisted with solid silicate: (1) at the smallest nanoscale fractures in silicate (Fig. 6C and D), (2) at the mesoscale in Portales Valley (Rubin et al., 2001; and Fig. 8A), (3) in the chondritic fragments in IAB iron meteorites (Fig. 8D), and (4) in pallasites, where troilite is invariably in contact with olivine and typically forms films between adjacent olivine crystals, whereas metal does not (the Brenham meteorite is an excellent example). Because sulfide-dominant melt appears to have migrated into chondritic clasts and vein margins at all scales of vein development, the entrainment of chondritic clasts in accumulations of molten metal is interpreted to promote purification of the metal. The wetting properties of sulfide melt allows chondritic clasts to act as sponges that soak up available sulfide via capillary action, removing chalcophile elements from the metal melt (e.g., see the sulfide-enriched chondritic clasts in NWA 5549; Fig. 8D). Presumably this would occur at the final stages of melt crystallisation, probably after impact-related deformation has ceased and when there may be some buoyancy-controlled separation of entrained silicate clasts from the metal (Fig. 10E).

4. CHEMICAL DISEQUILIBRIUM DURING MELTING AND MELT MIGRATION

4.1. Melt pocket formation (Stage 1)

Preferential melting of metal, and to a lesser extent FeS, over silicates, particularly olivine and pyroxene, during passage of an impact-associated shock wave occurs mainly because impact-induced heating is maximised at interfaces between high and low density phases (Stoffler et al., 1991). The greatest density contrast occurs between tetrataenite ($Fe_{50}Ni_{50}$: ρ of 8275 kg m^{-3}; low-Ni kamacite has ρ of 7900 kg m^{-3}) and pore spaces (see Stoffler et al., 1991), and then plagioclase ($\rho \approx 2680$ kg m^{-3}). Other large density contrasts occur at contacts between troilite ($\rho = 4610$ kg m^{-3}) and silicates. These density contrasts translate proportionately to shock impedance contrasts during impact events, with higher impedance contrasts resulting in greater heating (Stoffler et al., 1991). Thus, the grain boundary interfaces between FeNi metal and plagioclase are the focus of heating in preference to other phases. However, shock heating is dependant on the orientation of these grain boundaries with respect to the shock wave, and is maximised at orientations perpendicular to the shock front, which is why not all metal–plagioclase contacts, for example, are melted.

The combined requirement of high impedance contrast and perpendicular grain boundary orientation for maximised impact heating implies that heat generation will be highly spatially focussed. Fig. 2A shows an example of this, where high temperature taenite–tetrataenite melting (at ~1425 °C; the lower melt pocket) took place only 22 μm (possibly closer in the third dimension) away from an unmelted troilite–tetrataenite contact (the eutectic in the Fe_{50}-

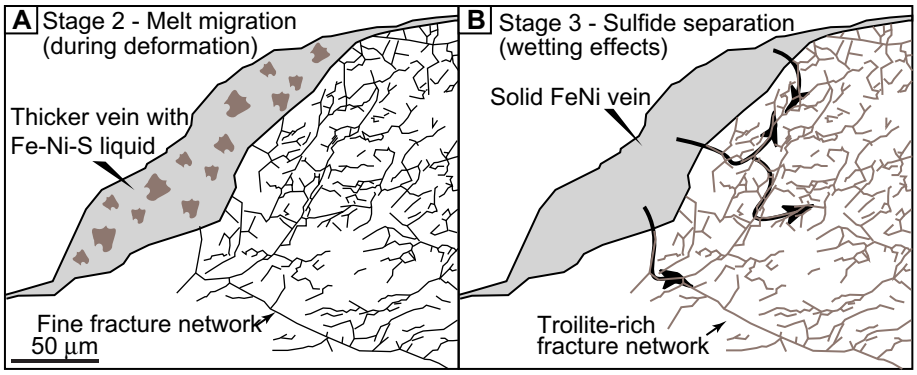

Fig. 11. Schematic representation of the evolution of sulfide separation from Fe–Ni–S accumulations. Panel (A) represents the situation at the end of deformation-driven segregation. Panel (B) represents the response to change in wetting behaviour of the melt as it cools towards the FeS-dominated eutectic composition; any permeable network in the silicate material generates a capillary pressure on wetting fluids, drawing FeS-rich melt away from the crystallising metal.

Ni_{50}–FeS system is at ~855 °C; see Tomkins, 2009), indicating extremely localised heating that created temperature gradients of at least 26 °C/μm. Clearly, the resulting melt pockets were not in thermochemical equilibrium with their surroundings, and therefore their compositions are not dominated by the FeNi–FeS eutectic, but instead vary considerably within the impact-affected volume. This was also suggested by Leroux et al. (2000). Our observations indicate that it is possible for FeNi–silicate, FeS–silicate and Fe-Ni + FeS–silicate melts to form independently of each other even at distances of <50 μm.

These small melt pockets would cool quickly and thus there should be little time for chemical equilibration between the residual metal and the melt. We tested this concept by comparing the Fe and Ni contents of residue and melt by electron microprobe element mapping. During chemical equilibration, Ni should preferentially partition into the melt from the residue metal (see Scott, 1972; Ni diffuses faster in FeNi metal than trace siderophile elements; Righter et al., 2005; see further discussion on diffusion rates below). Therefore our element maps, which record no enrichment in the melt of Ni over Fe (Fig. 2B–D), indicate chemical disequilibrium (see also Leroux et al., 2000). This is particularly so for the silicate-dominated emulsions, where metal/sulfide melt was almost instantaneously separated from its residue. Fig. 2B–D shows an example of how the chemistry of metal in melt pockets is controlled by mixing processes, rather than equilibrium-driven diffusion; here, metal derived from melting of Ni-rich taenite has partially mixed with metallic melt from kamacite, with distinct compositional domains preserved.

This incipient melting, with its heterogenous heat distribution, is the starting point of a series of processes involving periods of thermochemical disequilibrium. This initial disequilibrium condition is caused by the rapidity of the impact-induced pressure pulse that arrives during the contact and compression stage of crater development, which lasts from milliseconds to seconds (Stoffler et al., 1991). This melt formation mechanism is different to that associated with the subsequent rebound and collapse stages of crater development.

4.2. Melt vein and breccia formation (Stage 2)

From studies of impact craters on Earth we know that the later stages of crater formation generate spatially focused fault planes that experience extreme strain rates, which result in frictional melting along the plane of the fault and development of pseudotachylite (Melosh, 2005). On Earth this pseudotachylite can consist of a thin plane of silicate glass, or commonly, a dyke-like volume of rounded unmelted clasts cemented by glass. However, impact craters on Earth are different to those observed on asteroids in that on the former craters with diameters larger than ~4 km are complex craters with a central uplift, whereas on asteroids there are only simple craters, due mainly to the large differences in gravity (although see the Rheasilvia Impact Basin on Vesta). More prolonged and vigorous fault movement is associated with complex crater formation because of the uplift process. On Earth, large-scale rock faulting and frictional melting is thought to continue for several minutes for craters of 10–100 km diameter (Melosh, 2005). However, since impact craters on asteroids are likely to be considerably different to those on Earth (Keil et al., 1997; Rubin, 2005), the duration of violent fault movement associated with impacts may be considerably shorter, providing little time for chemical equilibration between melt and residue. Nevertheless, pseudotachylite-like impact melt veins and breccias (e.g., Fig. 4) are relatively common amongst the recovered meteorite population, and these extended melt zones would have promoted linking between the early-formed melt pockets.

The life spans of different melt volumes will vary greatly from seconds for the tiniest droplets that form in cold rocks near the surface of a planetesimal, to many years for the largest accumulations that are insulated within already warm rocks at depth in larger bodies (see Monteux et al., 2007). Since silicate rocks are excellent thermal insulators only the smaller melt domains can quench in the few minutes that impact deformation occurs over.

The diffusion rates of siderophile elements in kamacite show that impact events are too brief for equilibrium to be achieved between metal melt and residue metal

(although there are no published data for W and Hf). For example, the diffusion rate of Ni in kamacite is about 0.1 $\mu m^2 s^{-1}$ at 1400 °C and trace metals diffuse at the same rate as Ni or significantly slower (Righter et al., 2005). These authors indicate that diffusion of Ni in kamacite is about two orders of magnitude faster than in taenite. This may be fast enough for some diffusional equilibration to occur in places where molten metal stays in contact with residue kamacite for a period of longer than several tens of seconds (partial equilibration with taenite would take several tens of minutes); achievement of total equilibrium would take longer, varying as a function of grain size. However, the observed textures imply that molten metal in veins was separated from restitic metal almost instantaneously, thereby precluding all but the smallest degree of partial equilibration. The high closure temperature of the Hf–W system (for solid state diffusion between pyroxene and metal; Kleine et al., 2008) relative to that of Fe and Ni in metal indicates that W diffusion between silicate and metal is significantly more sluggish than Ni diffusion within metal. Thus, if Ni was not equilibrated in our observed examples, then neither will have W.

Electron microprobe analysis shows that in our samples there is no measurable chemical variability preserved between the melt phase and unmelted metal in areas where part of a metal grain can be seen to have melted and mobilised into a glassy silicate melt vein (e.g., Fig. 12). The melt was thus not enriched in incompatible siderophile elements relative to the residue metal, as it would be if chemical equilibration had occurred during melt separation. Therefore, the rapidity of melt migration was such that the small metal veins examined here formed under disequilibrium conditions. At larger scales, and/or at greater degrees of impact melting, the physical process driving melt migration is the same, so the rate of melt separation would be comparable, or faster if the impact event was larger. However, if a large fraction of melt was produced during a larger impact event, it is likely that unmelted components would be physically carried along by migrating melt; this would provide opportunity for some equilibration within the migrating melt–solid mixture.

4.3. The cooling period and melt crystallisation (Stage 3)

After deformation has ceased, melt accumulations that separated from their residue would be surrounded by unmelted regions at a range of scales, and the system would thermally equilibrate by radiative cooling. The amount of time that such a system remains partially molten is a function of the energy input, in that the larger the impact, the more energy in the system, and thus the longer the partially molten period. Furthermore, impacted regions that were already hot, from radiogenic metamorphism for example, would cool more slowly and stay molten for longer. There is also some indication that impact-induced melting can occur at considerable depths (e.g., Rubin et al., 2001; Ruzicka et al., 2005), and this insulated setting would also cool more slowly. This cooling period would have lasted considerably longer than the deformation period, in some cases orders of magnitude longer. Therefore, some chemical equilibration between metal and separating sulfide and silicate might be expected during this period; note that this is different to equilibration between the melt source and the melt accumulations. Furthermore, the differences in size and timing of impact events, and depth of melting, would have imparted considerable variability in the degree of chemical equilibrium achieved.

The quench textures between metal and troilite in melt pockets (e.g., Fig 1D) indicate that these would have had little time for chemical equilibration with surrounding or entrained silicate material as they cooled. However, the interpretation that troilite-dominated veinlets evolved during cooling of the melt towards a eutectic requires equilibration between metal and separating sulfide. The same applies to fractionation of troilite into chondritic fragments in Portales Valley and nonmagmatic iron meteorites. Elements that are chalcophile (e.g., Cu, and to some extent, Ni) should be depleted from the metal and enriched in the sulfide where these were able to separate. This is consistent with the observations of Portales Valley, which show that the sulfide-enriched silicate breccia clasts are also Cu-rich (Rubin et al., 2001). Elements that are siderophile (Ir, Os, Re in particular) will tend to be enriched in the metal by this process.

If some large metal–sulfide melt accumulations remain molten for long enough there may be time for gravitational separation of entrained silicate clasts. In this case there may be some chemical equilibration between metal and particularly smaller silicate particles (although smaller particles would be less efficiently separated), which would partition lithophile elements from the metal.

In systems where there was partial equilibration at some stage along the process of separating metal from silicate and sulfide, the separated metallic melt would have only partially partitioned the siderophile elements from the residue. The resulting siderophile element signature of such a metal melt would therefore be somewhere between an equilibrium melt and the residual metal composition. If one was modelling such a system by assuming equilibrium, the metal melt would look, chemically, like it had entrained some unmelted residual metal as it separated from the source, which is exactly the preferred model of Ruzicka et al. (2005) for the coarse metal veins of Portales Valley. Similarly, nonmagmatic IAB iron meteorites are best modelled as fractionating mixtures of solid residue metal and liquid metal in models that assume equilibrium partitioning (see Wasson and Kallemeyn, 2002). This suggests that the chemistry of Portales Valley and nonmagmatic iron meteorites could reflect variability in chemical disequilibrium developed during rapid impact-induced metal migration and subsequent cooling.

5. IMPLICATIONS FOR CORE FORMATION IN PLANETESIMALS

At the completion of the impact-related sequence of metal and sulfide melt migration processes, enlarged accumulations of relatively sulfide-free metal are left encapsulated in a volume of chondritic material that may be sulfide-enriched, and that may retain fine-grained unmobilised metal

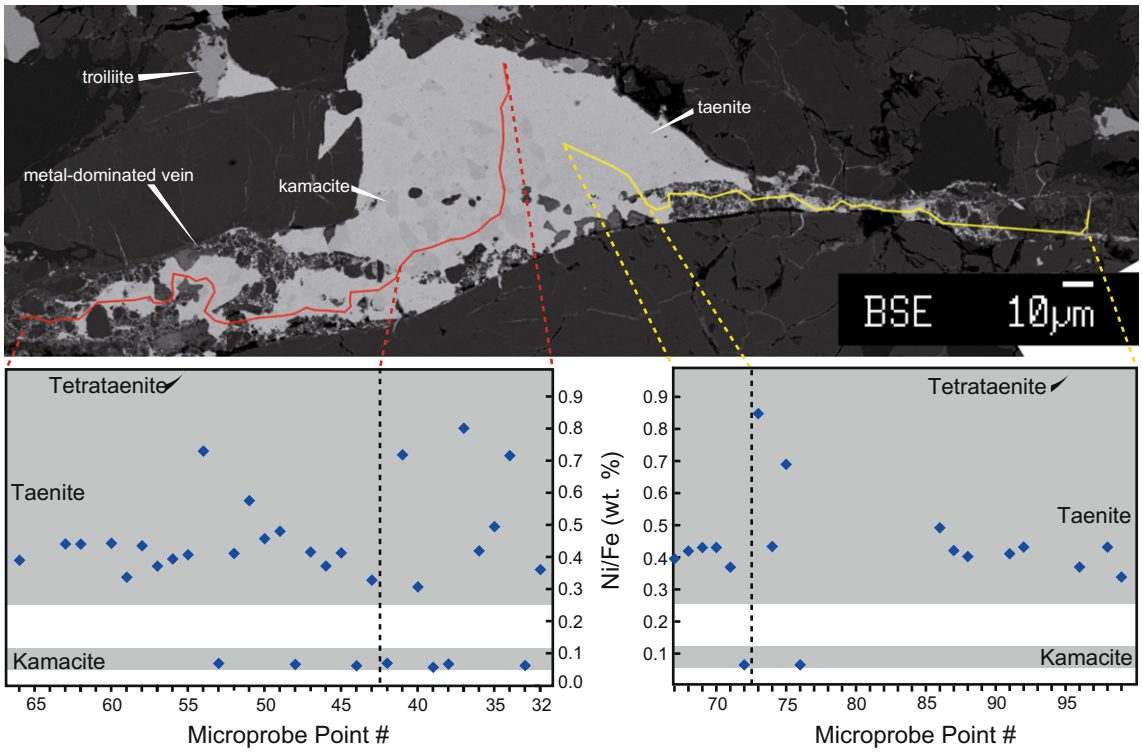

Fig. 12. Electron microprobe data traverses from residual unmelted metal into melted and mobilised metal in a melt vein in the La Criolla L6 ordinary chondrite. Below are plotted Fe/Ni ratios against distance for the traverses. The horizontal black lines on the graphed data show solid composition best fits, whilst the grey line shows extrapolations of these lines. The data show no evidence of fractionation between the residual metal grain and the melted and mobilised metal in the vein. Imaging as for Fig. 2A; data were collected using a JEOL 8500F CL HyperProbe operating at 12 kV and 16 nA.

particles. This process would have happened numerous times for each large body as they progressively grew to planetesimal size; with every impact large enough to generate significant melting. Some metal accumulations may have been very large; for example, the nonmagmatic iron meteorite that formed Meteor Crater in Arizona (Canyon Diablo) may have been on the order of 3×10^5 tonnes (Melosh and Collins, 2005).

Stokes Law indicates that the gravitational settling rate of metal particles towards a core through a molten or partially molten silicate mantle scales with the square of the metal particle diameter. Therefore, if enlarged FeNi metal accumulations were able to form within planetesimals prior to the onset of widespread silicate partial melting, these would be segregated far more rapidly to cores upon silicate melting than the small metal particles typical of chondritic meteorites. This contrast in settling potential is even greater between enlarged metal accumulations and fine troilite microfracture coatings.

The old ages of magmatic iron meteorites imply that radiogenic heating was critical to their formation, and that planetesimals needed to undergo widespread silicate partial melting for cores to form (cf. Bagdassarov et al., 2009). Before widespread partial melting could begin, planetesimals needed to grow large enough to insulate the required amount of heat generated by radioactive decay of ^{26}Al and ^{60}Fe (Moskovitz and Gaidos, 2011). As the apparent age of magmatic iron meteorites is within 1.5 million years of CAIs (Carlson and Boyet, 2009; Kruijer et al., 2012), this growth likely happened very rapidly, which implies that energetic collisions would have been a feature of this time. Thus, it is almost unavoidable that impact-driven FeNi segregation would have been occurring on some scale during this growth phase.

Settling of metal globules through a partially molten mantle in the time available on the largest asteroids requires globule sizes at least an order of magnitude larger than the typical metal grains found in chondrites (Scott, 1972), and this scales to several orders of magnitude on smaller planetesimals. This early work is consistent with the findings of (Bagdassarov et al., 2009), who showed experimentally that even the rate of percolative flow for Fe–S liquid through significantly partially melted peridotite was too slow by two orders of magnitude to form the core of Vesta in the time required by geochronology; again, the problem is greater for smaller asteroids. Impact-driven FeNi melt segregation provides a mechanism for early formation of larger metal accumulations with the gravitational potential needed to migrate rapidly to planetesimal cores upon widespread radiogenic silicate melting. Using a modified Hadamard–Rybczynski equation for settling of inviscid spheres ($V = 1/3[(\Delta\rho g r^2)/\eta]$; see Weinberg and Podladchikov, 1994) and the temperature and melt fraction corrected viscosity of peridotite with 26% melt from Bagdassarov

et al. (2009), we find that increasing the metal particle diameter to 2 m allows core formation on Vesta via settling in the time available. Since our study has identified a mechanism by which metal particle sizes are formed that can be considerably larger than this (some nonmagmatic iron meteorites represent larger bodies), we have identified a process that allows far more rapid core formation with less radiogenic heating. A further consideration is that the viscosity of molten peridotite drops by several orders of magnitude in the melt fraction (ϕ) range 0.25–0.30 (Scott and Kohlstedt, 2006), and so only moderately enlarged metal particles are needed when melting is this extensive. Although not well constrained, the data from these authors indicate that at $\phi = 0.30$ the bulk viscosity of molten peridotite is $<10^8$ Pa s; at this upper bound, metal particle sizes $>\sim$12 cm would settle to the core of Vesta in the time available, whereas FeS particles would need to be $>\sim$20 cm. At $\phi > 0.35$ peridotite bulk viscosity varies according to the Einstein–Roscoe equation ($\eta_{bulk} = \eta_{liq}(1.35\ \phi - 0.35)^{-2.5}$; Scott and Kohlstedt, 2006), such that when ϕ reaches 0.35, metal particle sizes $>\sim$500 μm would settle to the core of Vesta in the time available, whereas FeS particles would need to be $>\sim$900 μm (using $\eta_{liq} = 10$ Pa s; see Villeneuve et al., 2008). Given that we see metal grains in HED meteorites larger than 500 μm, core formation in Vesta likely proceeded at $\phi < 0.35$ (although the argument can be made that this is late veneer material; Day et al., 2012), in the range where the existence of large metal particles is needed for accelerated core formation.

Widespread settling of small metallic melt globules throughout a molten silicate body (i.e., the equilibrium-based model) would promote incorporation of a significant amount of FeS, possibly eutectic proportions (85% FeS). Cores that formed through this process would crystallise large masses of eutectic composition material, dominated by FeS, at the final stage of solidification. Thus, the rarity of troilite-rich and eutectic (FeNi–FeS) meteorites, and the comparative abundance of magmatic iron meteorites, has been seen as a significant paradox. The current explanation for this paradox suggests that the low resistance of troilite to space weathering, its high ablation-rate during passage through the atmosphere, and its high rate of weathering on the Earth's surface (although troilite weathers slower than FeNi metal in meteorites), combined to completely destroy these meteorites before they could be collected (Haack and McCoy, 2003). We have shown that the impact-driven melt segregation process involves removal of sulfide from enlarged metal accumulations at a range of scales. Once planetesimal mantles started to undergo widespread melting these enlarged metal accumulations would have significantly reduced capacity to chemically interact with their surroundings as they settled because; (1) the surface area to volume ratio of spherical globules diminishes with increasing radius (r) as a function of $3/r$, and (2) there is less time available for equilibration with surroundings during faster settling. The largest metal globules would therefore accumulate the lowest proportion of sulfide, and partition the least siderophile elements from their surroundings, during settling. Cores formed through this process would contain some sulfide, but would generate a comparatively small volume of eutectic composition liquid through fractional crystallisation. Thus, in contrast to existing equilibrium-based models of core formation, the observed rarity of sulfide-dominant meteorites is an expected consequence of our model.

A further possibility is that once the metal accumulations are sulfide depleted and have crystallised (i.e., shortly after impact-driven melt mobilisation), they will be relatively resistant to remelting (S-free FeNi metal melts at 1425 °C, whereas silicate melting starts at ~1150 °C), and so some metal accumulations may have settled to cores as largely solid masses rather than as liquids. The geochemistry of magmatic iron meteorites indicates that they crystallised from fractionating metallic melt (Scott and Wasson, 1975), but this does not constrain when or where the melt formed. Transfer of FeNi metal to cores would transfer radiogenic ^{60}Fe into a more insulated setting, and this would enhance core heating (Yoshino et al., 2003; Mostefaoui et al., 2005; Moskovitz and Gaidos, 2011), potentially promoting melting of solid components. If some metal migrated to cores in solid form, this would preclude equilibration between metal and silicate mantle.

If it is true that metal segregated to the cores of planetesimals under conditions of partial disequilibrium, then interpretations on the timing of core formation based on the Hf–W isotopic system (e.g., Carlson and Boyet, 2009) are incorrect. If there was no equilibration between metal and silicate mantle during core formation, metal would not be able to partition any of the ^{182}W that formed in silicates through decay of ^{182}Hf. In this case, the metal would contain only the initial ε^{182}W that it inherited from the solar nebula, and its isotopic age would be the same as CAIs. Fig. 4 in Kruijer et al. (2012) (see also Carlson and Boyet, 2009) shows that the ε^{182}W data of most magmatic iron meteorites are within error of the ε^{182}W of CAIs in Allende. We therefore suggest that the ε^{182}W data of magmatic iron meteorites are supporting evidence that the cores of planetesimals formed out of equilibrium with their mantles. Planetesimal cores must have formed rapidly and early, consistent with the necessarily short timescale of radiogenic heating and conductive cooling (Moskovitz and Gaidos, 2011), but we suggest that the ε^{182}W data should not interpreted as indicating core formation within 1.5 million years of CAIs because this model assumes equilibrium.

6. IMPLICATIONS FOR THE GEOCHEMISTRY OF PLANETARY MANTLES

Highly siderophile element abundances in the upper mantles of Earth and Mars are too high, by up to three orders of magnitude, for these mantles to have been in equilibrium with their cores (Taylor, 2001). By itself, the late veneer hypothesis (e.g., see Maier et al., 2009) does not adequately explain this problem because it requires plate tectonics to circulate late-accreting material into the Martian mantle since HSE in the Earth's upper mantle and the Martian mantle are broadly the same (Walker, 2009); a requirement in opposition with the observed lack of surface features consistent with subduction-related plate tectonics on Mars.

The timescale of radiogenic heating and conductive cooling for small bodies (Moskovitz and Gaidos, 2011) requires that plantesimal core formation was ubiquitously brief. Since gravitational settling rate scales with the square of metal particle size, small metal/sulfide particles would tend to be left behind while only enlarged metal accumulations settled rapidly enough, particularly in smaller bodies, to form cores in the short time windows available. Indeed, small metal and sulfide particles are relatively common in diogenites (e.g., Gooley and Moore, 1976), which represent samples from deep within the 525 km diameter asteroid Vesta (de Sanctis et al., 2012). These small metal particles, together with sulfide trapped in silicate material, would contain a considerable budget of highly siderophile elements (HSE). Accretion of these incompletely differentiated planetesimals, with HSE-rich mantles, would likely transfer some of this disequilibrium condition to planetary mantles (see Rudge et al., 2010; Rubie et al., 2011), potentially explaining their elevated HSE signatures. If this was the case, the consequences for the Hf–W isotope systematics of the Earth need to be considered. This idea is consistent with the observation that Earth's mantle siderophile element abundances are in approximately CI proportions (Taylor, 2001) in that equilibrium partitioning would change these ratios (Walker, 2009).

7. CONCLUSIONS

Impact events between asteroids and planetesimals cause metal, sulfide and silicate melting in a deformational environment. Through examining impact-related textures in ordinary chondrites we have shown that this deformation creates localised pressure gradients, which drives segregation of enlarged accumulations of Fe–Ni–S melt. The rapidity of this process means that the Fe–Ni–S melt separates from silicate material under conditions of thermochemical disequilibrium. As these accumulations cool towards FeS-dominated eutectic compositions, the liquid appears to change from having non-wetting to wetting properties against silicates, and this is interpreted to cause sulfide-rich melt to migrate away from metal into any permeable network in adjacent chondritic material. At the end of this process enlarged S-depleted FeNi accumulations, some possibly as large as many tonnes, are encapsulated within S-enriched silicate material.

This process should have proceeded as the earliest planetesimals grew by rapid collisional accretion. Once these bodies grew large enough to insulate the requisite radiogenic heat for silicate melting, the enlarged FeNi accumulations would migrate far more rapidly to cores than the small metal particles typical of chondritic meteorites because settling rate scales with the square of the particle diameter. In this way, at least some of the chemical disequilibrium that developed during deformation driven segregation would be transferred to planetesimal cores. Therefore, the isotopic models that assume equilibrium in the Hf–W system (see Carlson and Boyet, 2009) would underestimate the core formation time for any planetesimals that evolved by this process. Furthermore, unlike existing models of planetesimal core formation, this process would explain the relative lack of FeS-rich meteorites that should occur in our collections if equilibrium-based core formation was important.

ACKNOWLEDGMENTS

Museum Victoria is gratefully acknowledge for the loan of samples from the Etter, Hamilton, La Criolla and Talpa meteorites. We would like to thank in particular the Schmidt family for allowing us to collect meteorites on their property. Colin MacRae at the CSIRO Microbeam Laboratory is thanked for help with the electron microprobe work. Dr. Svend Buhl of Meteorite Recon is gratefully acknowledged for providing excellent photographs of the Chergach meteorite. Alex Ruzicka, Tracey Rushmer and an anonymous reviewer are thanked for helpful reviews, and Hiroko Nagahara is thanked for editorial handling and suggestions. Funding for this project was provided by a Monash Research Fellowship to A.G.T.

REFERENCES

Bagdassarov N., Solferino G., Golabek G. J. and Schmidt M. W. (2009) Centrifuge assisted percolation of Fe–S melts in partially molten peridotite: time constraints for planetary core formation. *Earth Planet. Sci. Lett.* **288**, 84–95.

Barnes S. J., Fiorentini M. L., Austin P., Gessner K., Hough R. M. and Squelch A. P. (2008) Three-dimensional morphology of magmatic sulfides sheds light on ore formation and sulfide melt migration. *Geology* **36**, 655–658.

Barnhoorn A., Cox S. F., Robinson D. J. and Senden T. (2010) Stress- and fluid-driven failure during fracture array growth: implications for coupled deformation and fluid flow in the crust. *Geology* **38**, 779–782.

Benedix G. K., McCoy T. J., Keil K. and Love S. G. (2000) A petrologic study of the IAB iron meteorites: constraints on the formation of the IAB-winonaite parent body. *Meteorit. Planet. Sci.* **35**, 1127–1141.

Bizzaro M., Baker J. A., Haack H. and Lundgaard K. L. (2005) Rapid timescales for accretion and melting of differentiated planetesimals infirred from ^{26}Al–^{26}Mg chronometry. *Astrophys. J.* **632**, L41–L44.

Bogard D. D., Garrison D. H. and McCoy T. J. (2000) Chronology and petrology of silicates from IIE iron meteorites: evidence of a complex parent body evolution. *Geochim. Cosmochim. Acta* **64**, 2133–2154.

Bonnet E., Bour O., Odling N. E., Davy P., Main I., Cowie P. and Berkowitz B. (2001) Scaling of fracture systems in geological media. *Rev. Geophys.* **39**, 347–383.

Britt D. T. and Consolmagno G. J. (2003) Stony meteorite porosities and densities: a review of the data through 2001. *Meteorit. Planet. Sci.* **38**, 1161–1180.

Bruhn D., Groebner N. and Kohlstedt D. L. (2000) An interconnected network of core forming melts produced by shear deformation. *Nature* **403**, 883–886.

Carlson R. W. and Boyet M. (2009) Short-lived radionuclides as monitors of early crust–mantle differentiation on the terrestrial planets. *Earth Planet. Sci. Lett.* **279**, 147–156.

Carrigan C. R. and Eichelberger J. C. (1990) Zoning of magmas by viscosity in volcanic conduits. *Nature* **343**, 248–251.

Casanova I., Graf T. and Marti K. (1995) Discovery of an unmelted H-chondrite inclusion in an iron meteorite. *Science* **268**, 540–542.

Chabot N. L. and Haack H. (2006) Evolution of asteroidal cores. In *Meteorites and the Earth Solar System II* (eds. D. S. Lauretta

and H. Y. J. McSween). University of Arizona Press, Tucson, pp. 747–771.

Choi B.-G., Ouyang X. and Wasson J. T. (1995) Classification and origin of IAB and IIICD iron meteorites. *Geochim. Cosmochim. Acta* **59**, 593–612.

Corgne A., Wood B. J. and Fei Y. (2008) C- and S-rich molten alloy immiscibility and core formation of planetesimals. *Geochim. Cosmochim. Acta* **72**, 2409–2416.

Cox S. F. (2005) Coupling between deformation, fluid pressures, and fluid flow in ore-producing hydrothermal systems at depth in the crust. In *Economic Geology 100th Anniversary Volume* (eds. J. W. Hedenquist, J. F. H. Thompson, R. J. Goldfarb and J. P. Richards). Society of Economic Geologists, Littleton, Colorado, pp. 39–76.

Day J. M. D., Walker R. J., Qin L. and Rumble, III, D. (2012) Late accretion as a natural consequence of planetary growth. *Nat. Geosci.* **5**, 614–617.

de Sanctis M. C., Ammannito E., Capria M. T., Tosi F., Capaccioni F., Zambon F., Carraro F., Fonte S., Frigeri A., Jaumann R., Magni G., Marchi S., McCord T. B., McFadden L. A., McSween H. Y., Mittlefehldt D. W., Nathues A., Palomba E., Pieters C. M., Raymond C. A., Russell C. T., Toplis M. J. and Turrini D. (2012) Spectroscopic characterization of mineralogy and its diversity across Vesta. *Science* **366**, 697–700.

Dobson D. P., Chrichton W. A., Vocadlo L., Jones A. P., Wang Y., Uchida T., Rivers M. L., Sutton S. and Brodholt J. P. (2000) In situ measurement of viscosity of liquids in the Fe–FeS system at high pressures and temperatures. *Am. Miner.* **85**, 1838–1842.

Dodd R. T. and Jarosewich E. (1979) Incipient melting in shock classification of L-group chondrites. *Earth Planet. Sci. Lett.* **44**, 335–340.

Fagereng A. (2011) Fractal vein distributions within a fault-fracture mesh in an exhumed accretionary melange, Chrystalls Beach Complex, New Zealand. *J. Struct. Geol.* **33**, 918–927.

Gaetani G. A. and Grove T. L. (1999) Wetting of mantle olivine by sulfide melt: implications for Re/Os ratios in mantle peridotite and late-stage core formation. *Earth Planet. Sci. Lett.* **169**, 147–163.

Gooley R. and Moore C. B. (1976) Native metal in diogenite meteorites. *Am. Miner.* **61**, 373–378.

Haack H. and McCoy T. J. (2003) Iron and stony-iron meteorites. In *Meteorites, Comets, and Planets* (ed. A. M. Davis). Elsevier, Oxford, pp. 325–345.

Harrison K. P. and Grimm R. E. (2010) Thermal constraints on the early history of the H-chondrite parent body reconsidered. *Geochim. Cosmochim. Acta* **74**, 5410–5423.

Hummel W. and Arndt J. (1985) Variation of viscosity with temperature and composition in the plagioclase system. *Contrib. Mineral. Petrol.* **90**, 83–92.

Johnston J. D. and McCaffrey K. J. W. (1996) Fractal geometries of vein systems and the variation of scaling relationships with mechanism. *J. Struct. Geol.* **18**, 349–358.

Keil K., Stoffler D., Love S. G. and Scott E. R. D. (1997) Constraints on the role of impact heating and melting in asteroids. *Meteorit. Planet. Sci.* **32**, 349–363.

Kleine T., Touboul M., Bourdon B., Nimmo F., Mezger K., Palme H., Jacobsen S. B., Yin Q.-Z. and Halliday A. N. (2009) Hf–W chronology of the accretion and early evolution of asteroids and terrestrial planets. *Geochim. Cosmochim. Acta* **73**, 5150–5188.

Kleine T., Touboul M., van Orman J. A., Bourdan B., Maden C., Mezger K. and Halliday A. N. (2008) Hf–W thermochronometry: closure temperature and constraints on the accretion and cooling history of the H chondrite parent body. *Earth Planet. Sci. Lett.* **270**, 106–118.

Kong P., Ebihara M. and Xie X. (1998) Reevaluation of formation of metal nodules in ordinary chondrites. *Meteorit. Planet. Sci.* **33**, 993–998.

Kring D. A., Hill D. H., Gleason J. D., Britt D. T., Consolmagno G. J., Farmer M., Wilson S. and Haag R. (1999) Portales Valley: a meteoritic sample of the brecciated and metal-veined floor of an impact crater on an H-chondrite asteroid. *Meteorit. Planet. Sci.* **34**, 663–669.

Kruijer T. S., Sprung P., Kleine T., Leya I., Burkhardt C. and Wieler R. (2012) Hf-W chronometry of core formation in planetesimals inferred from weakly irradiated iron meteorites. *Geochim. Cosmochim. Acta.* **99**, 287–304.

Lauretta D. S., Lodders K., Fegley B. J. and Kremser D. T. (1997) The origin of sulfide-rimmed metal grains in ordinary chondrites. *Earth Planet. Sci. Lett.* **151**, 289–301.

Lee L.-H. (1991) *Adhesive Bonding*. Plenum Press, p. 476.

Leroux H., Doukhan J.-C. and Guyot F. (2000) Metal–silicate interaction in quenched shock-induced melt of the Tenham L6-chondrite. *Earth Planet. Sci. Lett.* **179**, 477–487.

Maier W. D., Barnes S. J., Campbell I. H., Fiorentini M. L., Peltonen P., Barnes S.-J. and Smithies R. H. (2009) Progressive mixing of meteoritic veneer into the early Earth's deep mantle. *Nature* **460**, 620–623.

Manning C. E. and Ingebritsen S. E. (1999) Permeability of the continental crust – the implications of geothermal data and metamorphic systems. *Rev. Geophys.* **37**, 127–150.

McCoy T. J., Keil K., Scott E. R. D. and Haack H. (1993) Genesis of the IIICD iron meteorites: evidence from silicate-bearing inclusions. *Meteoritics* **28**, 552–560.

McCoy T. J., Mittlefehldt D. W. and Wilson L. (2006) Asteroid differentiation. In *Meteorites and the Early Solar System II* (eds. D. S. Lauretta and H. Y. McSween). University of Arizona Press, Tucson, pp. 733–745.

Melosh H. J. (2005) The mechanics of pseudotachylite formation in impact events. In *Impact Teconics* (eds. C. Koeberl and H. Henkel). Springer, Berlin, Heidelberg, New York, pp. 55–80.

Melosh H. J. and Collins G. S. (2005) Planetary science: Meteor Crater formed by low-velocity impact. *Nature* **434**, 157.

Miller J. M. and Wilson C. J. L. (2005) Stress controls on intrusion-related gold lodes: Wonga gold mine, Stawell, western Lachlan Fold Belt, southeastern Australia. *Econ. Geol.* **99**, 941–963.

Minarik W. G., Ryerson F. J. and Watson B. E. (1996) Textural entrapment of core-forming melts. *Science* **272**, 530–533.

Monteux J., Coltice C., Dubuffet F. and Ricard Y. (2007) Thermo-mechanical adjustment after impacts during planetary growth. *Geophys. Res. Lett.* **34**, L24201.

Moskovitz N. and Gaidos E. (2011) Differentiation of planetessimals and the thermal consequences of melt migration. *Meteorit. Planet. Sci.* **46**, 903–918.

Mostefaoui S., Lugmair G. W. and Hoppe P. (2005) Fe-60: a heat source for planetary differentiation from a nearby supernova explosion. *Astrophys. J.* **625**, 271–277.

Nimmo F. and Agnor C. B. (2006) Isotopic outcomes of N-body accretion simulation: constraints on equilibration processes during large impacts from Hf/W observations. *Earth Planet. Sci. Lett.* **243**, 26–43.

Nortje G. S., Rowland J. V., Spordli K. B., Blenkinsop T. G. and Rabone S. D. C. (2006) Vein deflections and thickness variations of epithermal quartz veins as indicators of fracture coalescence. *J. Struct. Geol.* **28**, 1396–1405.

Olsen E., Davis A., Clark R. S. J., Schultz L., Weber H. W., Clayton R., Mayeda T., Jarosewich E., Sylvester P., Grossman L., Wang M.-S., Lipschultz M. E., Steele I. M. and Schwade J. (1994) Watson: a new link in the IIE iron chain. *Meteoritics* **29**, 200–213.

Qin L., Dauphas N., Wadhwa M., Masarik J. and Janney P. E. (2008) Rapid accretion and differentiation of iron meteorite parent bodies inferred from ^{182}Hf–^{182}W chronometry and thermal modeling. *Earth Planet. Sci. Lett.* **273**, 94–104.

Reisner R. J. and Goldstein J. I. (2003) Ordinary chondrite metallography: Part 2. Formation of zoned and unzoned metal particles in relatively unshocked H, L, and LL chondrites. *Meteorit. Planet. Sci.* **38**, 1679–1696.

Righter K., Campbell A. J. and Humayun M. (2005) Diffusion of trace elements in FeNi metal: application to zoned metal grains in chondrites. *Geochim. Cosmochim. Acta* **69**, 3145–3158.

Roberts J. J., Kinney J. H., Siebert J. and Ryerson F. J. (2007) Fe–Ni–S melt permeability in olivine: implications for planetary core formation. *Geophys. Res. Lett.* **34**, L14306.

Rubie D. C., Frost D. J., Mann U., Asahara Y., Nimmo F., Tsuno K., Kegler P., Holzheid A. and Palme H. (2011) Heterogeneous accretion, composition and core–mantle differentiation of the Earth. *Earth Planet. Sci. Lett.* **301**, 31–42.

Rubin A. E. (1999) Formation of large metal nodules in ordinary chondrites. *J. Geophys. Res.* **104**, 30799–30804.

Rubin A. E. (2002) Smyer H-chondrite impact-melt breccia and evidence for sulfur vaporization. *Geochim. Cosmochim. Acta* **66**, 699–711.

Rubin A. E. (2005) What heated the asteroids?. *Sci. Am.* **292** 80–87.

Rubin A. E., Ulff-Moller F., Wasson J. T. and Carlson W. D. (2001) The Portales Valley meteorite breccia: evidence for impact-induced melting and metamorphism of an ordinary chondrite. *Geochim. Cosmochim. Acta* **65**, 323–342.

Rudge J. F., Kleine T. and Bourdon B. (2010) Broad bounds on Earth's accretion and core formation constrained by geochemical models. *Nat. Geosci.* **3**, 439–443.

Rushmer T. and Petford N. (2011) Microsegregation rates of liquid Fe–Ni–S metal in natural silicate–metal systems: a combined experimental and numerical study. *Geochem. Geophys. Geosyst.* **12**, Q03014.

Rushmer T., Petford N., Humayun M. and Campbell A. J. (2005) Fe-liquid segregation in deforming planetesimals: coupling core-forming compositions with transport phenomena. *Earth Planet. Sci. Lett.* **239**, 185–202.

Ruzicka A. and Hutson M. (2010) Comparative petrology of silicates in the Udei Station (IAB) and Miles (IIE) iron meteorites: implications for the origin of silicate-bearing irons. *Geochim. Cosmochim. Acta* **74**, 394–433.

Ruzicka A., Killgore M., Mittlefehldt D. W. and Fries M. D. (2005) Portales Valley: petrology of a metallic-melt meteorite breccia. *Meteorit. Planet. Sci.* **40**, 261–295.

Sahijpal S., Soni P. and Gupta G. (2007) Numerical simulations of the differentiation of accreting planetesimals with ^{26}Al and ^{60}Fe as the heat sources. *Meteorit. Planet. Sci.* **42**, 1529–1548.

Sasso M. R., Macke R. J., Boesenberg J. S., Britt D. T., Rivers M. L., Ebel D. S. and Friedrich J. M. (2009) Incompletely compacted equilibrated ordinary chondrites. *Meteorit. Planet. Sci.* **44**, 1743–1753.

Schersten A., Elliott T., Hawkesworth C., Russell S. and Masarik J. (2006) Hf–W evidence for rapid differentiation of iron meteorite parent bodies. *Earth Planet. Sci. Lett.* **241**, 530–542.

Scott E. R. D. (1972) Chemical fractionation in iron meteorites and its interpretation. *Geochim. Cosmochim. Acta* **36**, 1205–1236.

Scott E. R. D. and Wasson J. T. (1975) Classification and properties of iron meteorites. *Rev. Geophys. Space Phys.* **13**, 527–546.

Scott T. and Kohlstedt D. L. (2006) The effect of large melt fraction on the deformation behavior of peridotite. *Earth Planet. Sci. Lett.* **246**, 177–187.

Shimoji M. and Itami T. (1986) *Atomic Transport in Liquid Metals*. TransTech Publications, Aedermansdorf, Switzerland.

Slater-Reynolds V. and McSween H. Y. (2005) Peak metamorphic temperatures in type 6 ordinary chondrites: an evaluation of pyroxene and plagioclase geothermometry. *Meteorit. Planet. Sci.* **40**, 745–754.

Stevenson D. J. (1990) Fluid dynamics of core formation. In *Origin of the Earth* (eds. H. E. Newsom and J. H. Drake). Oxford University Press, New York.

Stoffler D., Keil K. and Scott E. R. D. (1991) Shock metamorphism of ordinary chondrites. *Geochim. Cosmochim. Acta* **55**, 3845–3867.

Taylor S. R. (2001) *Solar System Evolution: A New Perspective*, second ed. Cambridge University Press, Cambridge.

Tomkins A. G. (2009) What metal–troilite textures can tell us about post-impact metamorphism in chondrite meteorites. *Meteorit. Planet. Sci.* **44**, 1133–1149.

Villeneuve N., Neuville D. R., Boivin P., Bachelery P. and Richet P. (2008) Magma crystallization and viscosity: a study of molten basalts from the Piton de la Fournaise volcano (La Réunion Island). *Chem. Geol.* **256**, 242–251.

Walker R. J. (2009) Highly siderophile elements in the Earth, Moon and Mars: update and implications for planetary accretion and differentiation. *Chem. Erde* **69**, 101–125.

Wasson J. T. and Kallemeyn G. W. (2002) The IAB iron meteorite complex: a group, five subgroups, numerous grouplets, closely related, mainly formed by crystal segregation in rapidly cooled melts. *Geochim. Cosmochim. Acta* **66**, 2445–2473.

Wasson J. T. and Richardson J. W. (2001) Fractionation trends among IVA iron meteorites: contrasts with IIIAB trends. *Geochim. Cosmochim. Acta* **65**, 951–970.

Wasson J. T. and Wang J. (1986) A nonmagmatic origin of group-IIE iron meteorites. *Geochim. Cosmochim. Acta* **50**, 725–732.

Wasson J. T., Willis J., Wai C. M. and Kracher A. (1980) Origin of iron meteorite groups IAB and IIICD. *Z. Naturforsch.* **35**, 781–795.

Weinberg R. F. and Podladchikov Y. (1994) Diapiric ascent of magmas through power-law crust and mantle. *J. Geophys. Res.* **99**, 9543–9559.

Widom E., Rubin A. E. and Wasson J. T. (1986) Composition and formation of metal nodules and veins in ordinary chondrites. *Geochim. Cosmochim. Acta* **50**, 1989–1995.

Wood B. J., Walter M. J. and Wade J. (2006) Accretion of the Earth and segregation of its core. *Nature* **441**, 825–833.

Yoshino T., Walter M. J. and Katsura T. (2003) Core formation in planetesimals triggered by permeable flow. *Nature* **422**, 154–157.

Yoshino T., Walter M. J. and Katsura T. (2004) Connectivity of molten Fe alloy in peridotite based on in situ electrical conductivity measurements: implications for core formation in terrestrial planets. *Earth Planet. Sci. Lett.* **222**, 625–643.

Associate editor: Hiroko Nagahara